Electronic Supplementary Material (ESI) for Journal of Materials Chemistry A.

Supporting Information for

Rapid, selective capture of toxic oxo-anions of Se(IV), Se(VI) and As(V) from water by an ionic metal-organic framework (iMOF)

Shivani Sharma,[a] Sumanta Let,[a] Aamod V. Desai,[a] Subhajit Dutta,[a] Gopalsamy Karuppasamy,[b] Mandar M. Shirolkar,[c] Ravichandar Babarao[b,d,e] and Sujit K. Ghosh*[a]

[a] Department of Chemistry, Indian Institute of Science Education and Research (IISER), Pune, Dr. Homi Bhabha Road, Pashan, Pune.

[b] School of Science, RMIT University, Melbourne, Melbourne 3001, Australia.

[c] Symbiosis Center for Nanoscience and Nanotechnology (SCNN), Symbiosis International (Deemed University) (SIU), Lavale, Pune 412115, Maharashtra, India

[d] Commonwealth Scientific and Industrial Research Organization (CSIRO) Manufacturing, Clayton, Victoria 3169, Australia

[e] Technische Universität Dresden, Theoretische Chemie, Bergstr,66c, 01062, Dresden, Germany

Corresponding author e-mail : sghosh@iiserpune.ac.in

EXPERIMENTAL PROCEDURES

Materials:

All solvents and reagents were commercially available and used without further purification. All experiments were performed at ambient temperature and Milli-Q water was utilized. Linker (L) (Scheme 1) was synthesized utilizing previous reported protocol.[1] ***Arsenic and selenium salts are toxic in nature and proper protective gear (masks, gloves) is always to be used***.

Synthesis of iMOF-3C:

Solvothermal reaction of linker L (8.86 mg, 0.02 mmol) and $NiSO_4 \cdot xH2O$ (8.42 mg, 0.03 mmol) in a solvent combination of DMF:water (2:1) was performed in a teflon lined vessel and heated at 130 °C for 48 h and then was cooled down to ambient temperature over 12 h. Hexagonal shaped crystals were separated from mother liquor by filtration and washed with DMF, water to remove any unreacted precursors followed by drying in air. Yield ~8.8 mg; % yield with respect to linker ~62%. Elemental Analysis: Calc. - C/H- 15.31 ; C/N- 3.30 ; C/S - 10.11 ; Found C/H- 15.18; C/N- 3.23; C/S- 10.1

For capture studies, the pristine MOF was exchanged with MeOH for 24h and thereafter activated in vacuum and was utilized as it is for capture experiments.

Stability studies of iMOF-3C:

For PXRD, FT-IR studies 30 mg of iMOF-3C was exposed 30 ml of different pH solution conditions including pH = 4, pH = 7, pH = 9 and pH =10 for 12 h and 10 days respectively. The solid samples were filtered and were used for measurements. For ICP spectroscopic analysis: 2 mg compound was exposed to 2 ml solution of various pH conditions including pH = 4, pH = 7, pH = 9 and pH =10. After 12 h and 10 days, dispersed solutions were centrifuged and solution was taken out and Ni(II) content was analyzed by ICP spectroscopy which would correspond to any decomposition.

Uptake of oxoanions of Se(IV)/Se(VI)/As(V)

All sorption experiments of iMOF-3C for oxoanions of Se(IV)/Se(VI)/As(V) were performed at room temperature. Aqueous solutions of oxoanions (50 ppm-1000 ppm) of Se(VI)/ Se(IV)/As(V) were prepared by dissolving their corresponding salts Na_2SeO_3, Na_2SeO_4, $Na_2HAsO_4.7H_2O$ in milli-Q water. The uptake studies were performed by batch experiments wherein 2 mg of iMOF-3C was dispersed in 2 ml (V/m = 1000 mL/g) aqueous solution of oxoanions of Se(VI)/Se(IV)/As(V) and the mixture was stirred in vortex to ensure maximum contact. After 24 h, the solutions were centrifuged and solutions were diluted further with 2-3% HNO_3 acid solution for ICP spectroscopic analysis. The ICP measurements were performed three times.

The adsorption capacity was determined by the following formula[2]: $Q = (C_o - C_f) \times V/m$ where C_o and C_f are the initial and final concentration of elements in solution, V is the volume of solution and m is the mass of sorbent material. The sorption isotherm was fitted using Langmuir isotherm model[3] with the following equation:

(1) Langmuir adsorption Model: Mathematical equation: $q_e = q_m (K_L C_e/(1+ KLC_e)$ wherein q_e represents equilibrium sorption capacity in mg/g, q_m represents theoretical maximum sorption capacity with monolayer coverage, K_L represents langmuir constant (L/mg), C_e represents the equilibrium concentration.

Sorption kinetics of iMOF-3C towards oxoanions of Se(IV)/Se(VI)/As(V)

Sorption kinetics experiments was performed by exposing 5 mg of iMOF-3C to 5 ml of 10 ppm aqueous solution of oxoanions of Se(IV)/Se(VI)/As(V). The solutions were stirred on vortex to ensure sufficient contact time. At specific intervals ranging from 10 min to 1800 min, suspensions were centrifuged for 2 mins at 7800 rpm and were diluted with 2-3% HNO_3 acid solution for further analysis by ICP spectroscopy.

The kinetics data was fitted with different kinetic model[3] using the following equations:

(1) Pseudo first order kinetic model:

$\ln(q_e - q_t) = \ln q_e - k_1 t.$

(2) Pseudo Second order kinetic model:

$t/q_t = 1/K_2 q_e^2 + t/q_e$

wherein q_e is the amount adsorbed by sorbent after equilibration, q_t is the amount adsorbed by sorbent at time t, K_1 (min^{-1}) and K_2 (g/mg min^{-1}) is the equilibrium rate constants of pseudo first order and second order rate constant.

Low concentration (1 ppm) kinetic experiments were performed by exposing 6 mg of iMOF-3C to 6 ml aqueous solution of Se(IV)/Se(VI)/As(V) respectively. The solutions were stirred on vortex to ensure sufficient contact time and at specific time intervals ranging from 2 min-180 min, and 24 h. Further, the suspensions were centrifuged for 2 min at 7800 rpm. The solution was taken out and were analyzed further using ICP spectroscopy.

The % removal was calculated by the following equation: $100\ \% \times (C_o - C_f)/ C_o$. The distribution coefficient (K_d) was calculated based on the following equation[3] $[\{(C_o - C_f) / C_f) \times V\}/m]$.

Low concentration kinetics of iMOF-3C towards mixture of oxoanions of Se(IV)/Se(VI)/As(V)

Stock solution was prepared with effective concentration of Se(IV)/Se(VI)/As(V) ~1 ppm and ~10 ppm each. 6 mg of iMOF-3C was exposed to 6 ml aqueous solution containing mixture of Se(IV)/Se(VI)/As(V). The solutions were stirred on vortex to ensure sufficient contact time and after 24 h, the suspensions were centrifuged for 2 min at 7800 rpm. The solution was taken out and were analyzed further using ICP spectroscopy.

Competing ion studies of iMOF-3C towards capture of oxoanions of Se(IV)/Se(VI)/As(V) in presence of Cl^-, NO_3^-, SO_4^{2-}, CO_3^{2-}

Competing ion experiments was performed by exposing 2 mg of iMOF-3C to 2 ml solution containing 1 ml of 20 ppm aqueous solution of oxoanions of Se(IV)/Se(VI)/As(V) and 1 ml 20 ppm solution of Cl^-, NO_3^-, SO_4^{2-}, CO_3^{2-} with an effective concentration ~ 10 ppm. The solutions were stirred on vortex to ensure sufficient contact time and after 24 h, suspensions were centrifuged for 2 min at 7800 rpm and were diluted with 2-3% HNO_3 acid solution for further analysis by ICP spectroscopy.

For higher concentrations of competing ion, 2 mg of iMOF-3C was exposed to 1 ml of 10 ppm solution of respective aqueous solution of Se(IV)/Se(VI)/As(V) and 1 ml aqueous solution of SO_4^{2-}, CO_3^{2-} at higher concentration ratios of 100 ppm ,1000 ppm and 10000 ppm. After 24 h, the solutions were centrifuged and were diluted with 2-3% HNO_3 acid solution for further analysis by ICP spectroscopy.

Real-time stability test for oxoanion of Se(IV), Se(VI) and As(V)

The solid samples exposed to various pH conditions for 10 days were further tested for their capability to capture oxoanions of Se(IV), Se(VI) and As(V). For this 2mg of exposed samples as well as pristine samples were exposed to 2 ml of toxic oxoanion solution containing mixture of Se(IV), Se(VI) and As(V) at two different concentrations of 1000 ppb and 10 ppm each. The solutions were stirred on vortex for 24 h to ensure sufficient contact time and after 24 h, suspensions were centrifuged for 2 min at 7800 rpm and solution was further analysis by ICP spectroscopy. The uptake performance of iMOF-3C was compared against pristine samples under the same conditions.

Uptake towards oxoanions of Se(IV), Se(VI) and As(V) in real-time conditions

For real-time analysis, Mutha river water (From Pune, India) was spiked with 1000 ppb of Se(IV)/Se(VI)/As(V) each. 6 mg of iMOF-3C to 6 ml of this spiked solution. The solutions were stirred on vortex for 24 h to ensure sufficient contact time and after 24 h, suspensions were centrifuged for 2 min at 7800 rpm and solution was further analysis by ICP spectroscopy.

Physical Measurements

Powder X-ray diffraction patterns were recorded on Bruker D8 Advanced X-Ray diffractometer using Cu Kα radiation (λ= 1.5406 Å) in 5° to 40° 2θ range with a scan speed of 1.2° min^{-1}. The IR Spectra were acquired by using NICOLET 6700 FT-IR spectrophotometer using KBr pellet in 400-4000 cm^{-1} range. Transmission electron microscopy (TEM) images and high resolution TEM (HRTEM) images are captured by using a UHR FEG-TEM, JEOL JEM 2200FS field emission transmission electron microscope operated at 200 kV. The SEM images & EDX data were obtained using FEI Quanta 3D dual beam ESEM. Thermogravimetric analysis profiles were recorded on Perkin-Elmer STA6000, TGA analyzer under N_2 atmosphere with heating rate of 10 °C/min. ICP-AAS analysis were performed on Thermo Scientific iCE 3000 Series. ICP-MS was performed on Quadrupole inductively coupled plasma mass spectrometry (Q-ICP MS;

Thermo Scientific iCAP Q) instrument. ICP-AES analysis was performed on ARCOS, Simultaneous ICP Spectrometer. Multi-element standards were purchased from in-organic ventures. X-ray Photoelectron Spectroscopy (XPS) studies were performed using K-Alpha+ model (Thermo Fischer Scientific, UK) with Al Kα source (λ = 1486.7 eV). The XPS spectra were corrected considering carbon C1s spectrum as standard. The standard peak position of C1s was taken at 284.6 eV and accordingly each element specific scans (short/high – resolution scans) were corrected. The data fitting was done using XPSPEAK41 software. During fitting Shirley background was considered and peak shape was optimized by appropriately adjusting Gaussian to Lorentzian ratio.

X-ray Structural Studies:

Single-crystal X-ray data of compound iMOF-3C was collected at 100 K on a Bruker D8 Venture Duo X-ray diffractometer equipped with Microfocus X-ray source (operated at 50 W; 50 kV/1 mA), graded multilayer optics for monochromatic Mo Kα radiation (λ = 0.71073 Å) focused X-ray beam and Photon 100 CMOS chip-based detector system. Crystal was mounted on nylon CryoLoops (Hampton Research) with Paraton-N (Hampton Research). The data integration and reduction were processed with SAINT soft-ware.[4] A multi-scan absorption correction was applied to the collected reflections.[5] The structure was solved by the direct method using SHELXTL[6-7] and was refined on F2 by full-matrix least-squares technique using the SHELXL-2014/7[8] program package within the WINGX[9] programme. All non-hydrogen atoms were refined anisotropically. All hydrogen atoms were located in successive difference Fourier maps and they were treated as riding atoms using SHELXL default parameters. The structures were examined using the Adsym subroutine of PLATON to assure that no additional symmetry could be applied to the models. The SQUEEZE option[10] was used to eliminate the contribution of disordered guest molecules and sulphate anions.

CCDC 1990643 (iMOF-3C) contains the supplementary crystallographic data for this paper. These data can be obtained free of charge from The Cambridge Crystallographic Data Centre via www.ccdc.cam.ac.uk/data_request/cif.

DFT calculations:

Periodic geometric optimization and the static binding energies for each anion in iMOF-3C frameworks were calculated using density functional theory (DFT) as implemented in the software package VASP 5.4.4.[11] It is well-known that standard DFT methods based on generalized gradient approximation do not fully account for the long-range dispersion interactions between the framework and the bound adsorbates. To accurately estimate static binding energies for each ani-on with the framework, we implemented dispersion corrections using DFT-D3 method[12]. Electron exchange and correlation were described using the generalized gradient approximation Perdew, Burke, and Ernzerhof (PBE)[13] form and the projector-augmented wave potentials were used to treat core and valence electrons[14]. In all cases, we used a plane-wave kinetic energy cutoff of 800 eV and a Gamma-point mesh for sampling the Brillouin zone. The ionic coordinates were relaxed until the Hellman-Feynman ionic forces were less than 0.01 eV/Å. The lattice parameters were fixed at the experimental values.

Electrostatic Potential Surface (ESP):

Density functional theory (DFT) computations were performed using the Gaussian program[15] to derive the ESP surface of iMOF-C3 cluster model. Based on the periodic DFT optimized structure of iMOF-C3, two different cluster models which contains one Ni2+ cation and six linkers were constructed. Each linker contains one imidazole ring and one benzene ring and the terminal sp^3 carbon atom of each linker was saturated by H atoms. Geometry optimization of fragment were carried out in the liquid phase at (SMD)B3LYP-D3/SDD~6-31G(d) level. The SMD implicit solvent model[16] with water as the solvent was used to include the solvation effects. The hybrid B3LYP exchange-correlation functional[17-18] combined with the D3 version of Grimme's dispersion[19] were employed. The Stuttgart/Dresden relativistic effective core potential and the associated valence basis set (SDD) were applied for Ni[20-21], while the 6-31G(d) basis sets were used for C, H, O, and N[22]. During optimizations, the Ni^{2+} cations, the N and C atoms of the imidazole rings, and the terminal sp^3 carbons were fixed. The electrostatic potential (ESP) on the van der Waals (VDW) surfaces (isodensity = 0.001 a.u.) of iMOF-3C fragment was derived based on its ground state electron density.

Simulated Annealing:

The lowest energy configuration of each anions in the primitive cell of iMOF-C3 MOF structure was obtained from the classical simulated annealing technique using classical force field as implemented in sorption module in Materials Studio.[23] The framework atoms are kept frozen during simulation. The interactions of gas-adsorbent and gas-gas were modeled as a combination of pairwise site-site Lennard-Jones (LJ) and Coulombic potentials. The LJ potential parameters of both the framework atoms and the adsorbates are adopted from the Universal force field (UFF).[24] The charges for the framework atoms were as-signed based on the Qeq charges as implemented in Materials Studio package. DFT optimization was per-formed on each anion using Dmol3 [23] module. The Becke exchange plus Lee-Yang-Parr correlation functional and all-electron core potentials were used. The double-ξ numerical polarization (DNP) basis set was adopted, which is comparable to the 6-31G(d,p) Gaussian type basis set. The DNP basis set incorporates d-type polarization into heavier atoms and p-type polarization into hydrogen atoms. Electrostatic potential charges were assigned to each anion based on the DFT optimised model.

In the simulated annealing method, the temperature was lowered stepwise, allowing the gas molecule to reach a desirable configuration based on different moves such as rotation, translation and repositioning with pre-set probabilities of occurrence. This process of heating and cooling the system was repeated in several heating cycles to find the local minima. Forty heating cycles were performed where the maximum temperature and the final temperature were 10^5 K and 100 K, respectively.

Binding Energies:

The initial location of the anion in the primitive cell of iMOF-C3 was obtained from the classical simulated annealing technique as described above. Static binding energies (ΔE) at 0 K in vacuum were calculated using the following expression

$$\Delta E = E_{(MOF+Anion)} - E_{(MOF+)} - E_{Anion}$$

where E_x refers, respectively, to the total energies of the MOF + Anion complex, the charged MOF+ alone, and the anion molecule respectively.

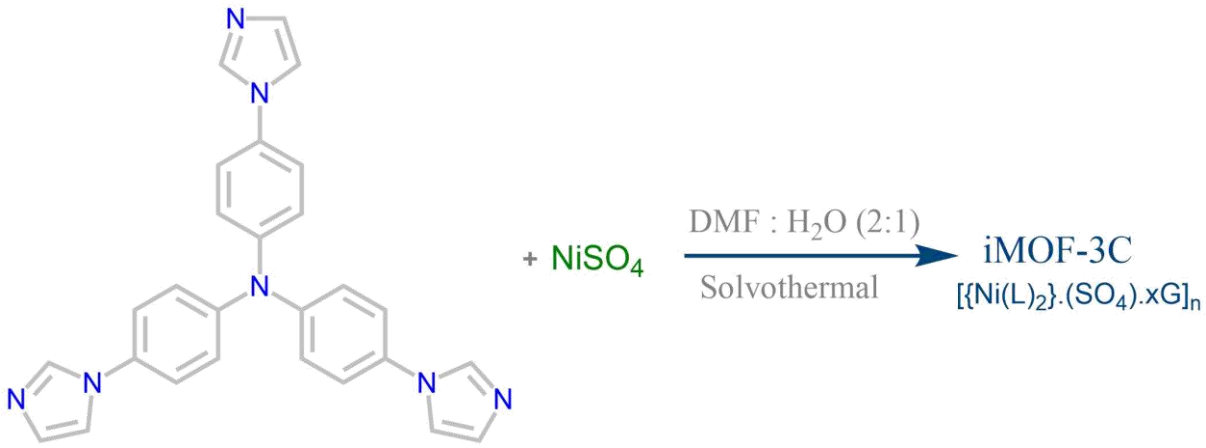

FigureS1: Schematic representation showing synthesis for iMOF-3C.

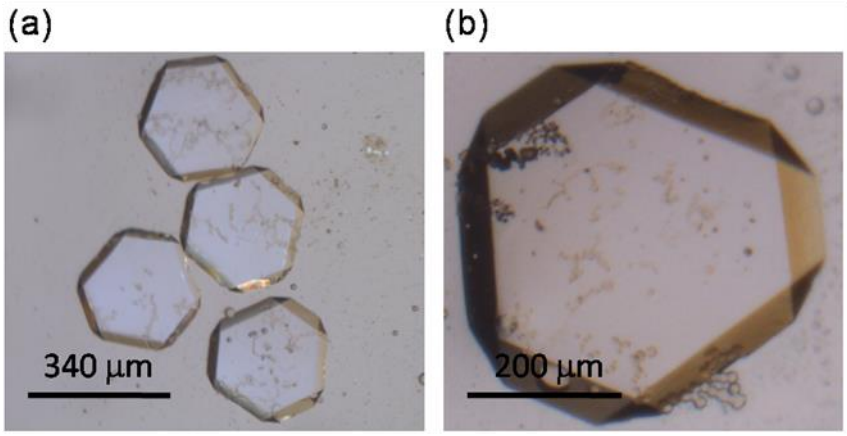

Figure S2: Photographs of parent framework viz. iMOF-3C, a) Bulk and b) single crystal under optical microscope.

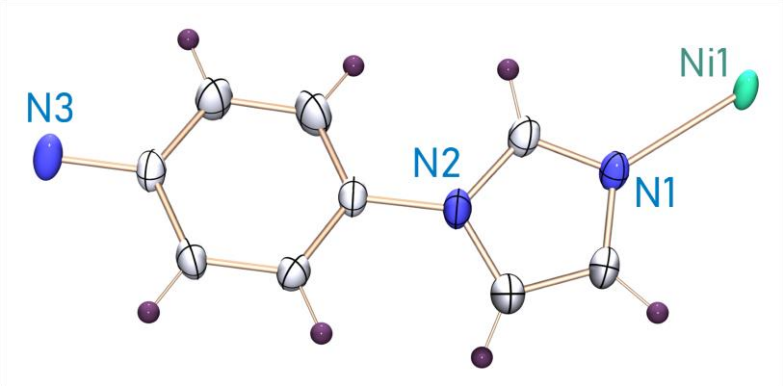

Figure S3: ORTEP diagram of asymmetric unit of pristine MOF.

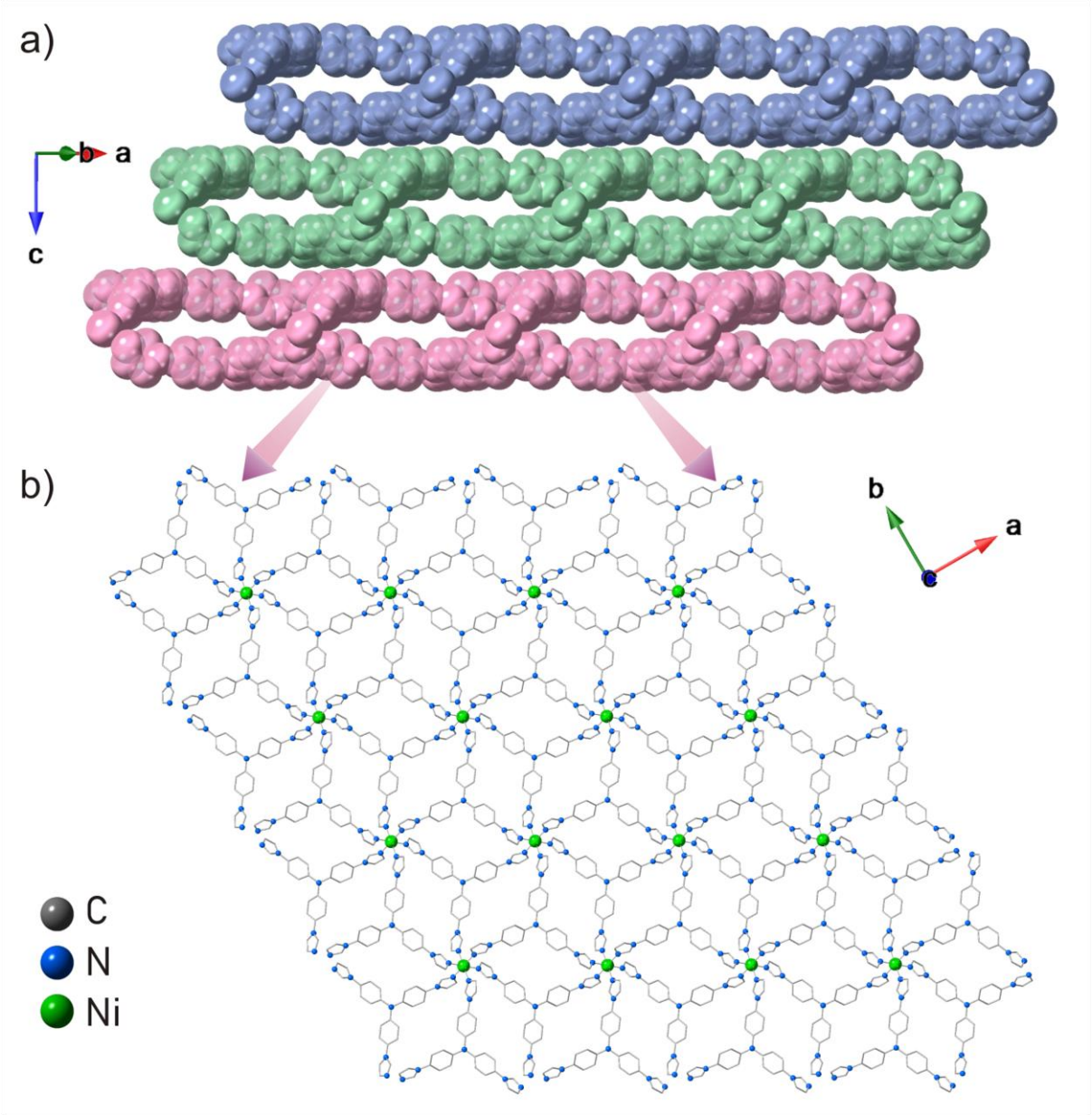

Figure S4: Packing diagram showing two dimensional layered structure of iMOF-3C and a single net showing coordination of linker(L) with Ni(II) nodes.(H-atoms omitted for clarity).

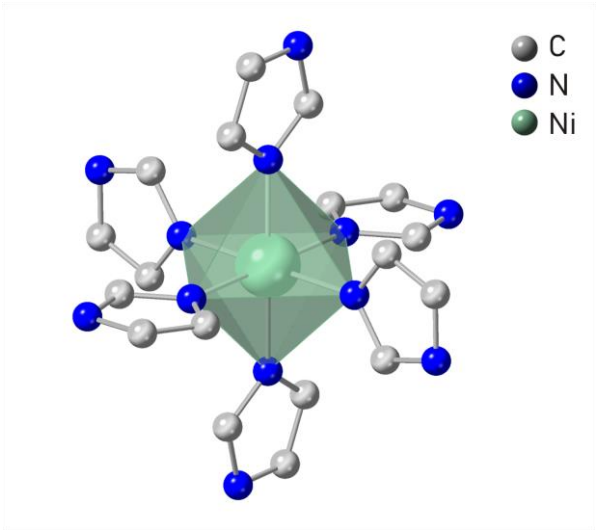

Figure S5: Coordination environment of the Ni(II) metal center.

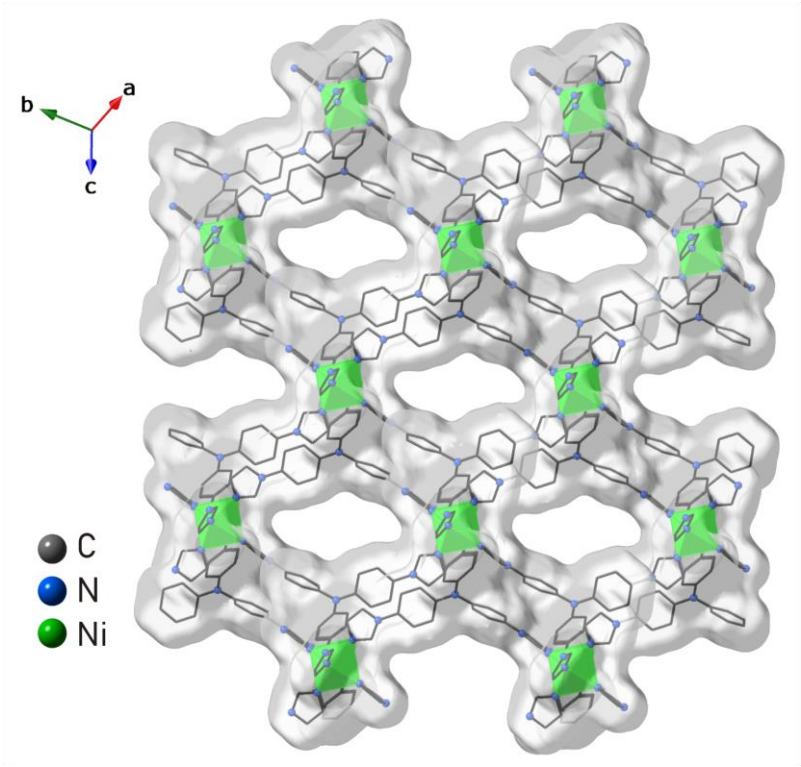

Figure S6: Packing diagram depicting one dimensional porous voids.(Disordered SO_4^{2-} anions, hydrogen atoms and solvent have been omitted for clarity).

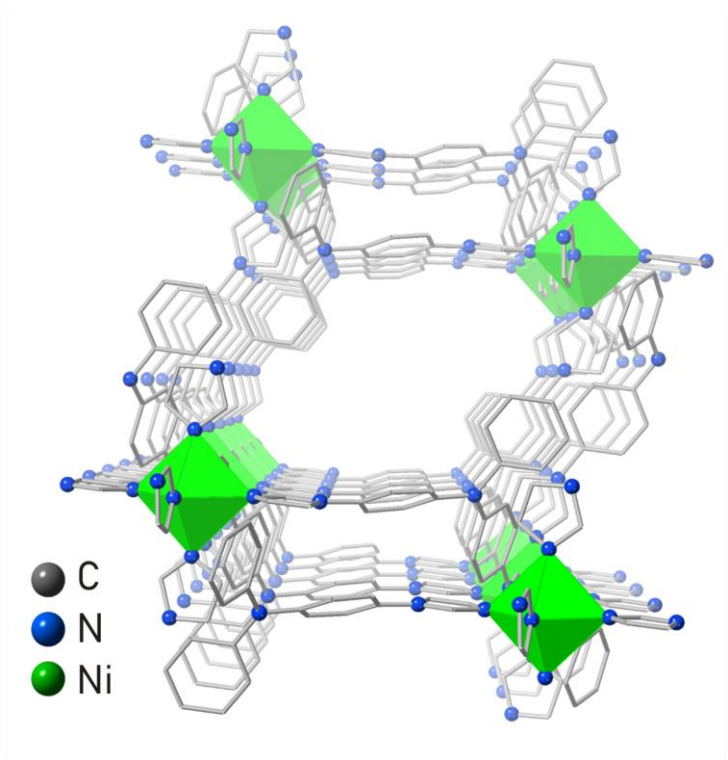

Figure S7: Packing diagram showing aperture of the porous channels. (Disordered SO_4^{2-} anions, hydrogen atoms and solvent have been omitted for clarity). The dimension of the voids excluding the Van der Walls radii is 6.6 × 4.89 Å^2.

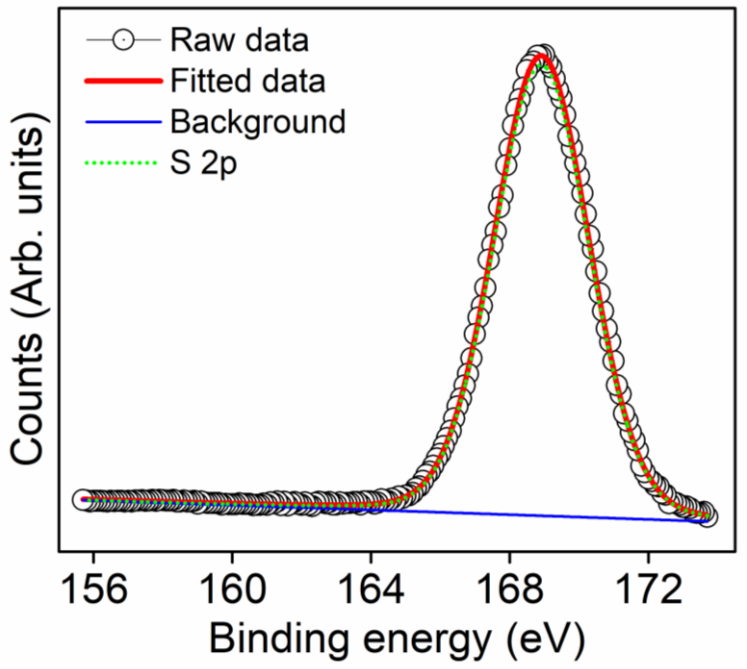

Figure S8: XPS fitting profile for sulphur (S 2p) in iMOF-3C.

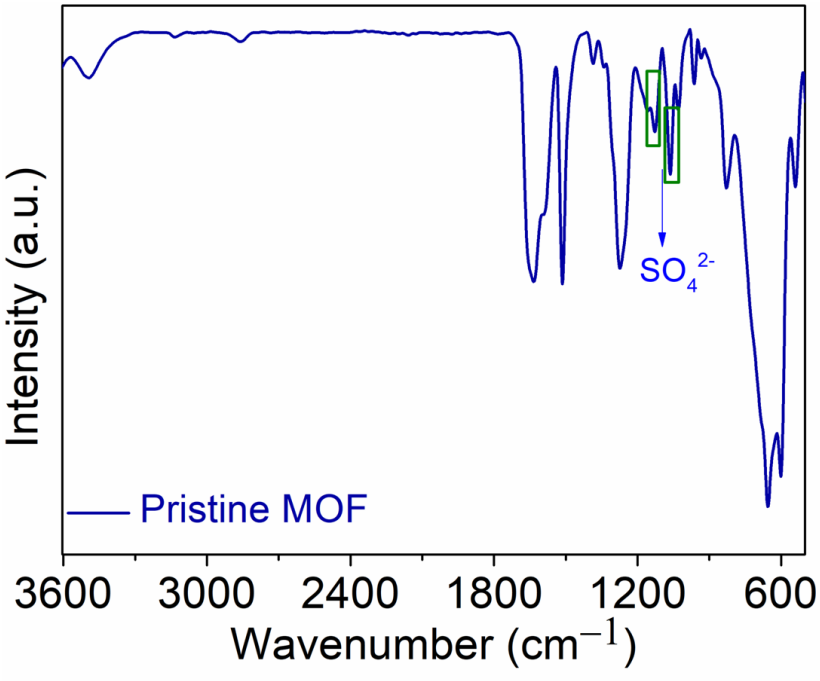

Figure S9: FT-IR spectra for pristine iMOF-3C showing peak corresponding to SO_4^{2-} anion.

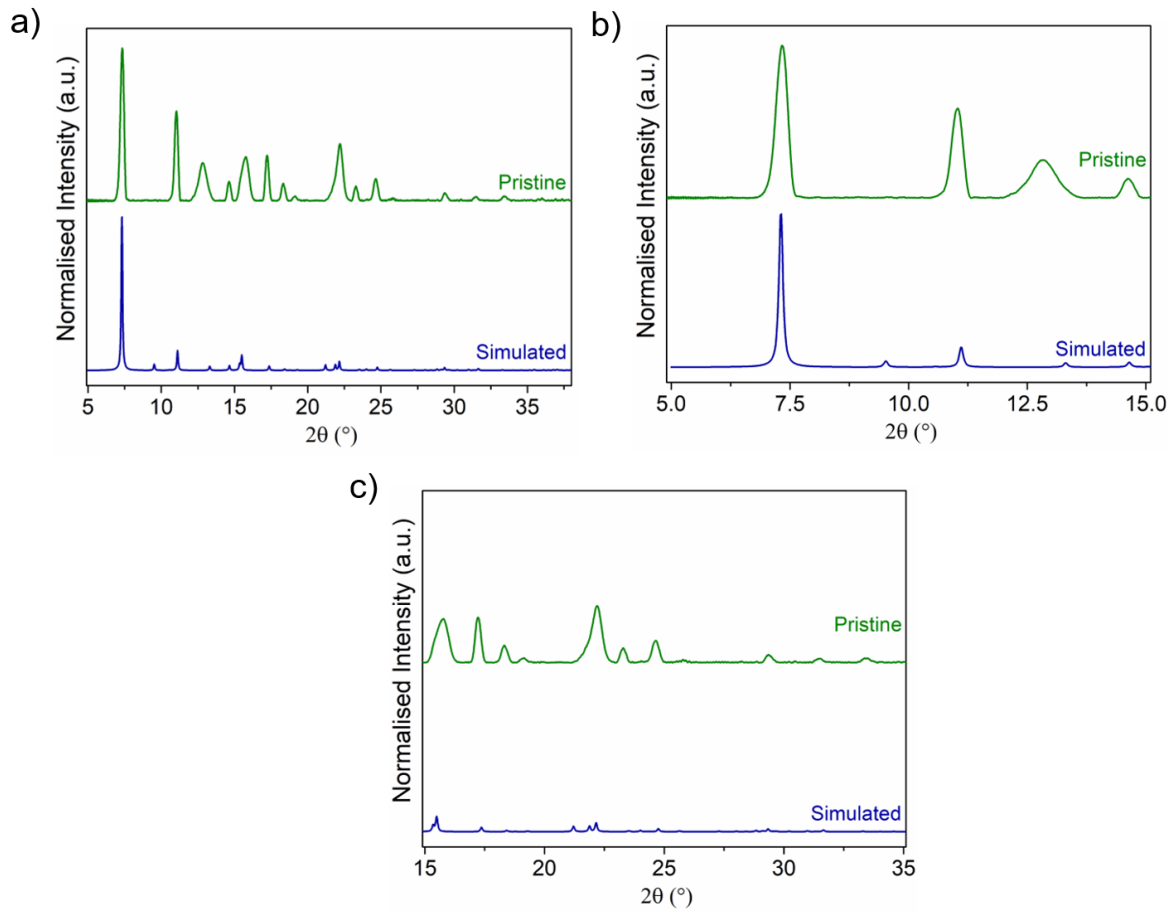

Figure S10: (a) PXRD spectra for simulated and pristine iMOF-3C. (b), (c): Zoomed view of the PXRD spectra.

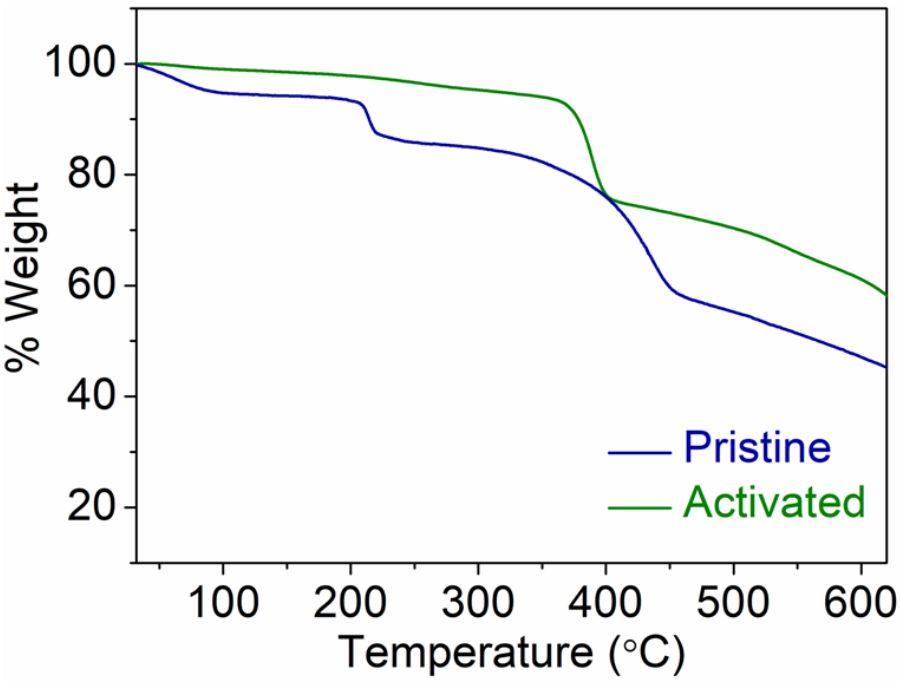

Figure S11: Thermogravimetric analysis for pristine iMOF-3C.

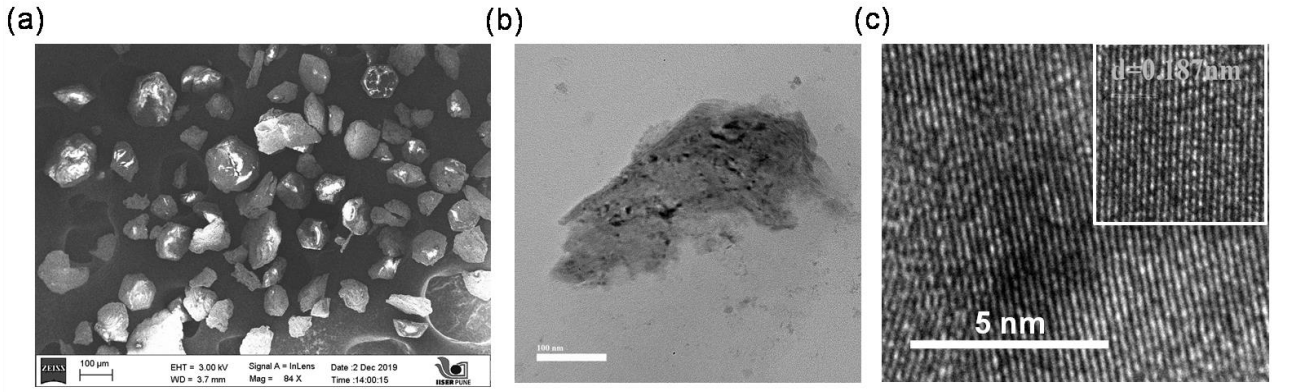

Figure S12: FESEM, TEM, HRTEM (Lattice fringes) images for pristine iMOF-3C.

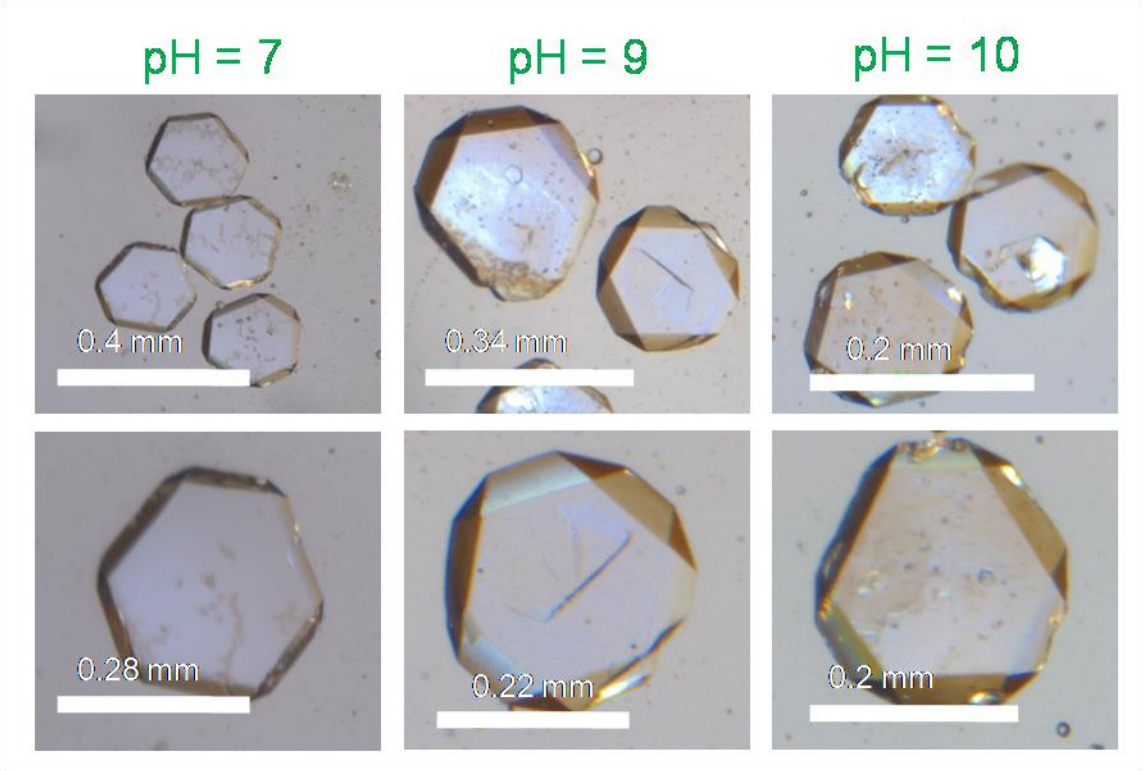

Figure S13: Optical microscopy images of pristine iMOF-3C dipped in various media.

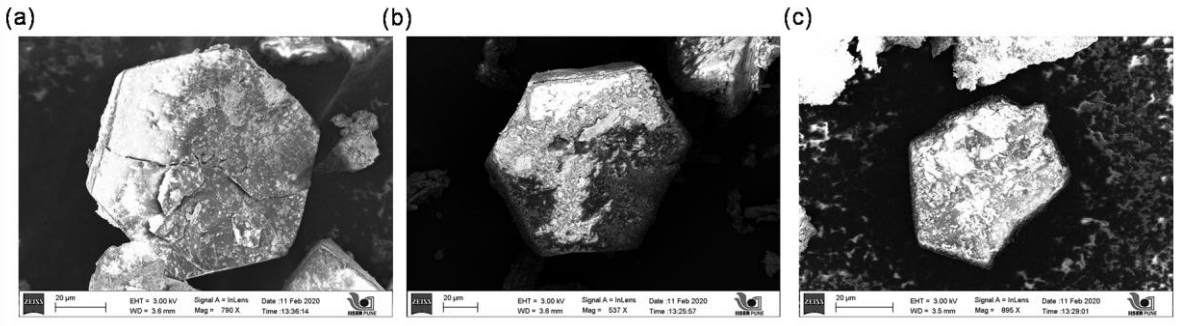

Figure S14: FESEM images of pristine iMOF-3C post-treatment in various media for 12 h (a) pH=7, pH=9, pH=10.

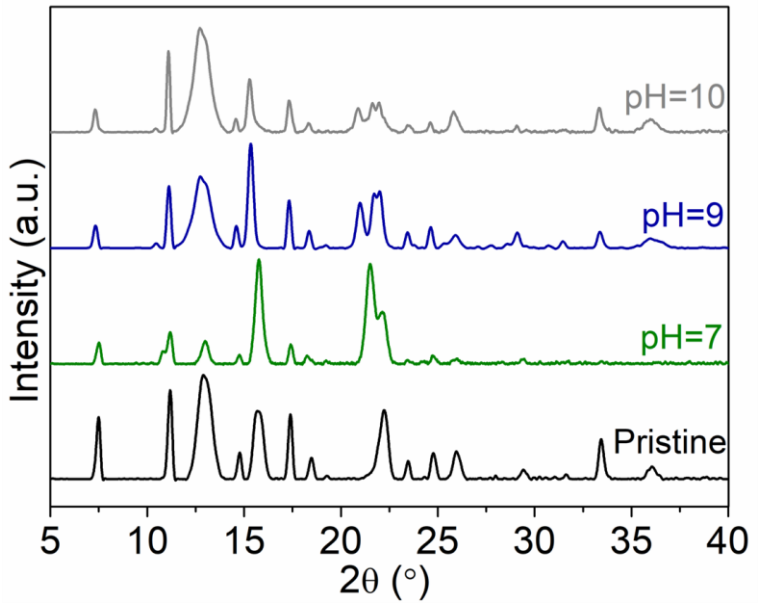

Figure S15: PXRD spectra of pristine iMOF-3C post-treatment in various media for 12 h.

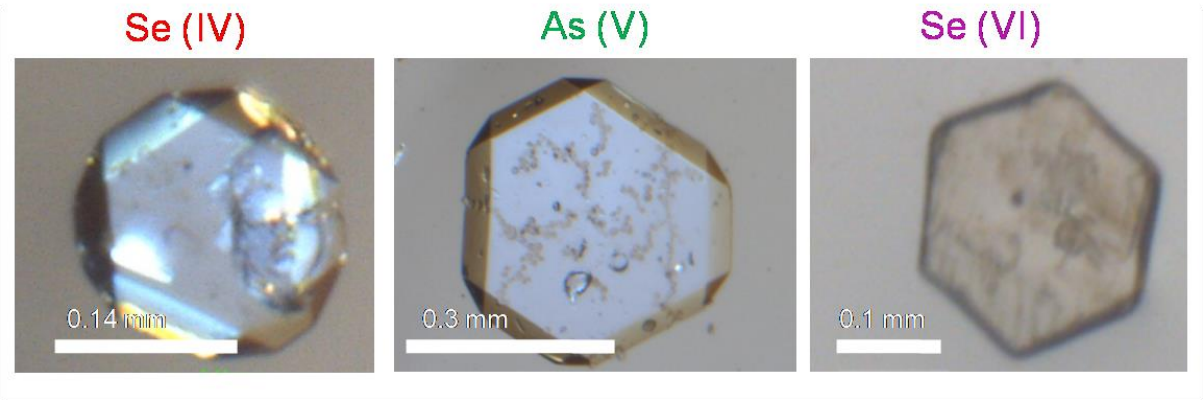

Figure S16: Optical microscopy images of pristine iMOF-3C dipped in aqueous solution of toxic oxo-anions viz. SeO_3^{2-}, SeO_4^{2-}, $HAsO_4^{2-}$.

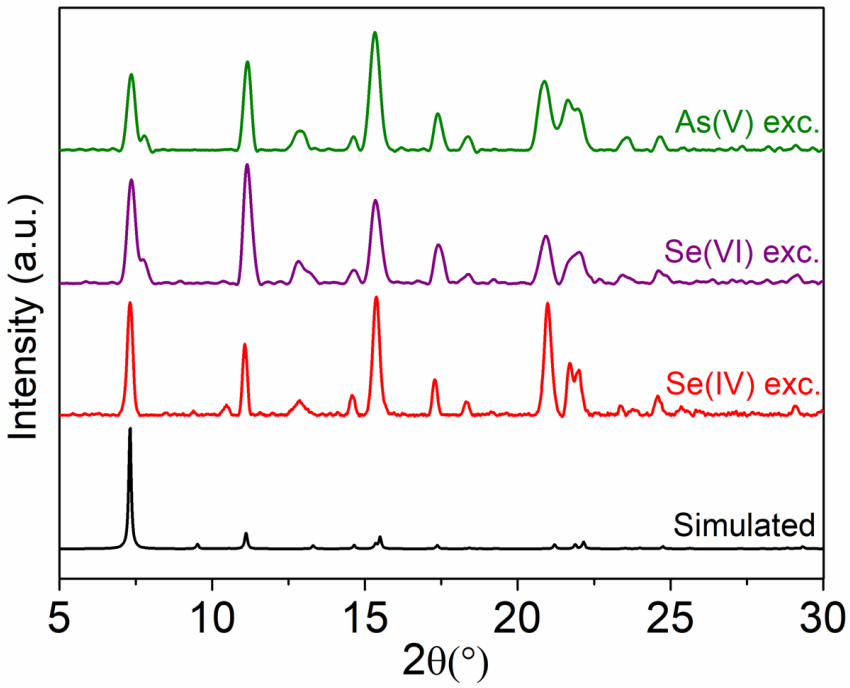

Figure S17: PXRD spectra for simulated iMOF-3C, pristine and SeO_3^{2-}, SeO_4^{2-}, $HAsO_4^{2-}$exchanged phases.

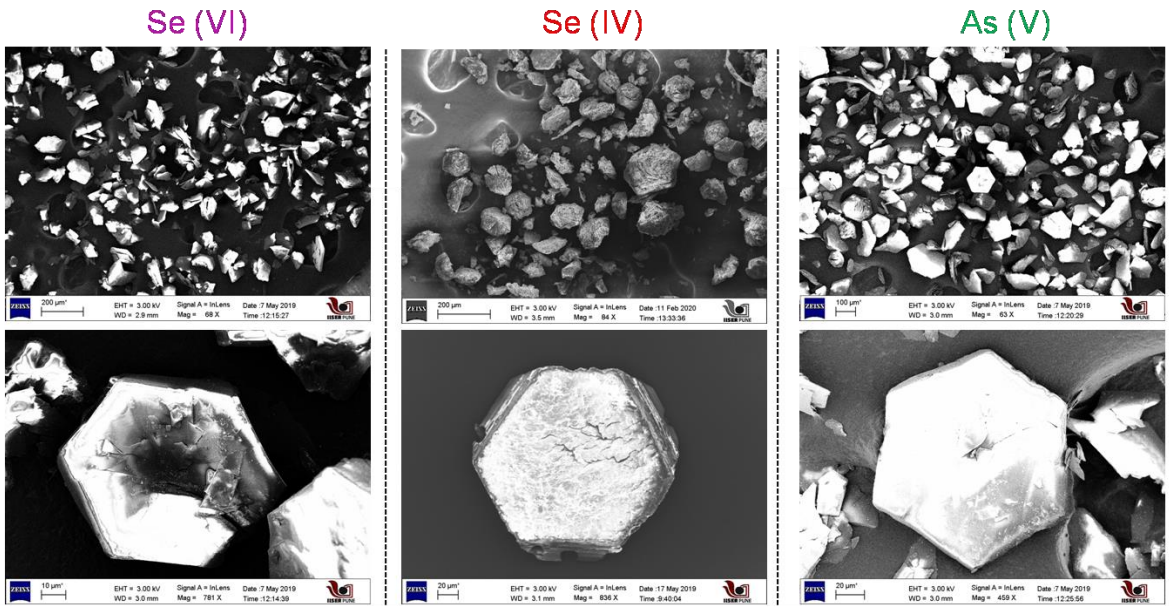

Figure S18: FESEM images for pristine MOF exposed to an aqueous solution of SeO_3^{2-}, SeO_4^{2-}, $HAsO_4^{2-}$.

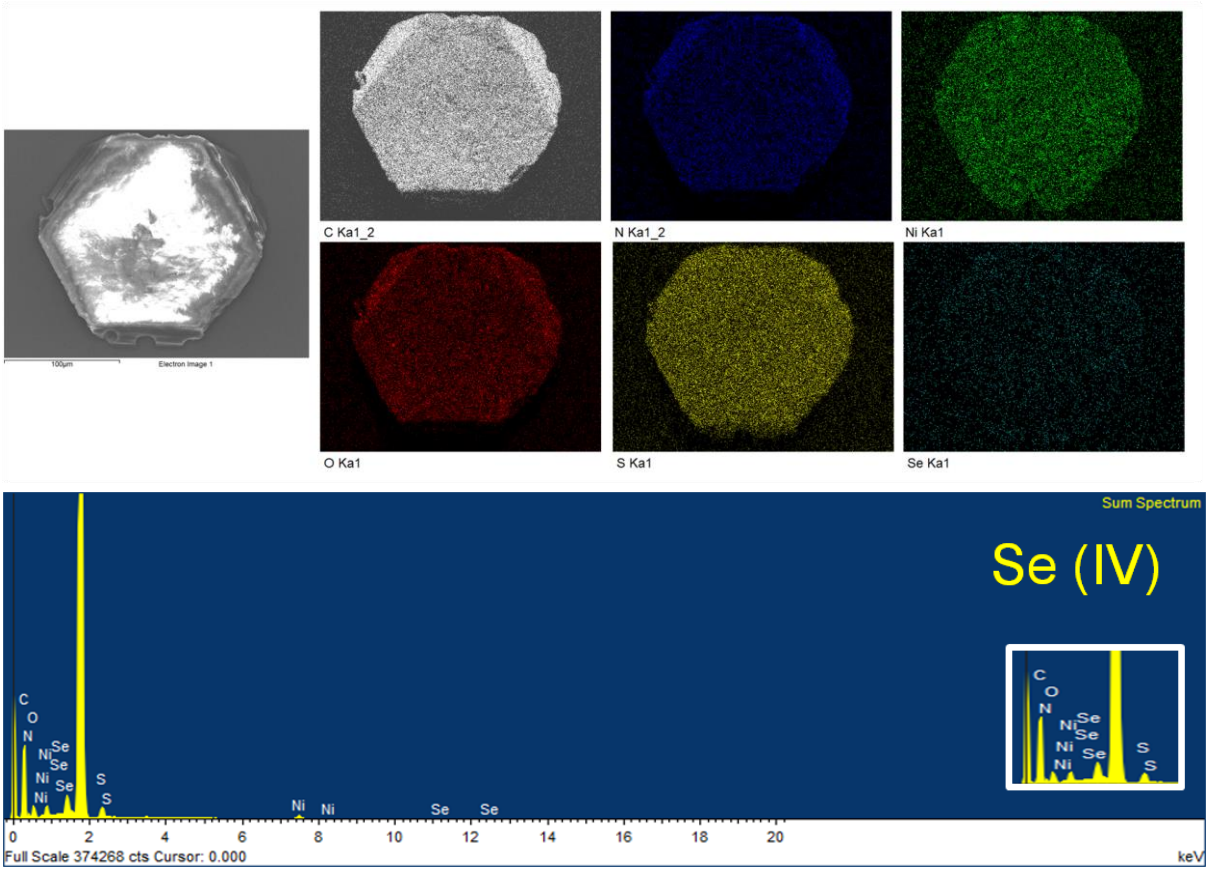

Element	Atomic %
C	65.32
N	17.12
O	14.91
S	0.86
Ni	0.88
Se	0.91

Figure S19: EDX mapping profile and spectra for pristine MOF exposed to an aqueous solution of SeO_3^{2-}.

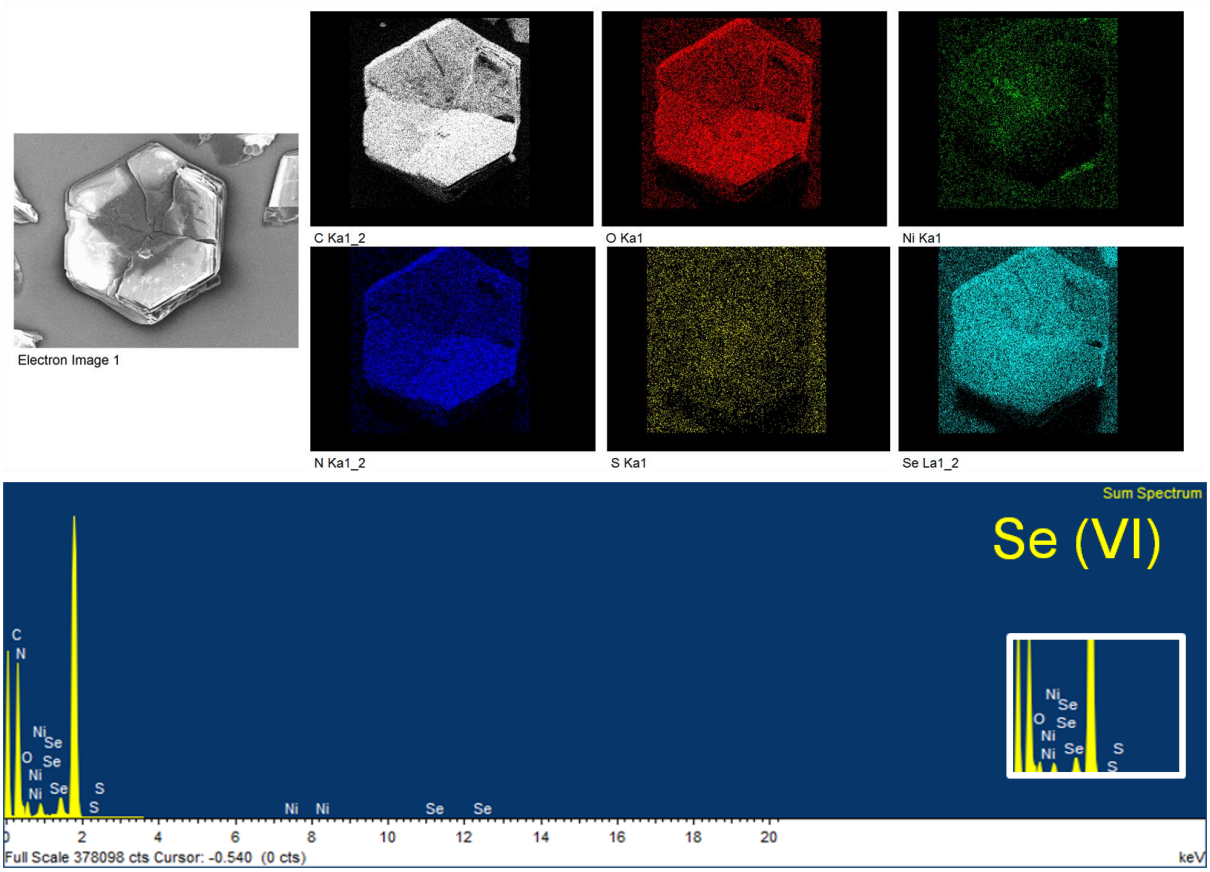

Element	Atomic %
C	64.08
N	22.54
O	12.08
S	0.06
Ni	0.47
Se	0.78

Figure S20: EDX mapping profile and spectra for pristine MOF exposed to an aqueous solution of SeO_4^{2-}.·

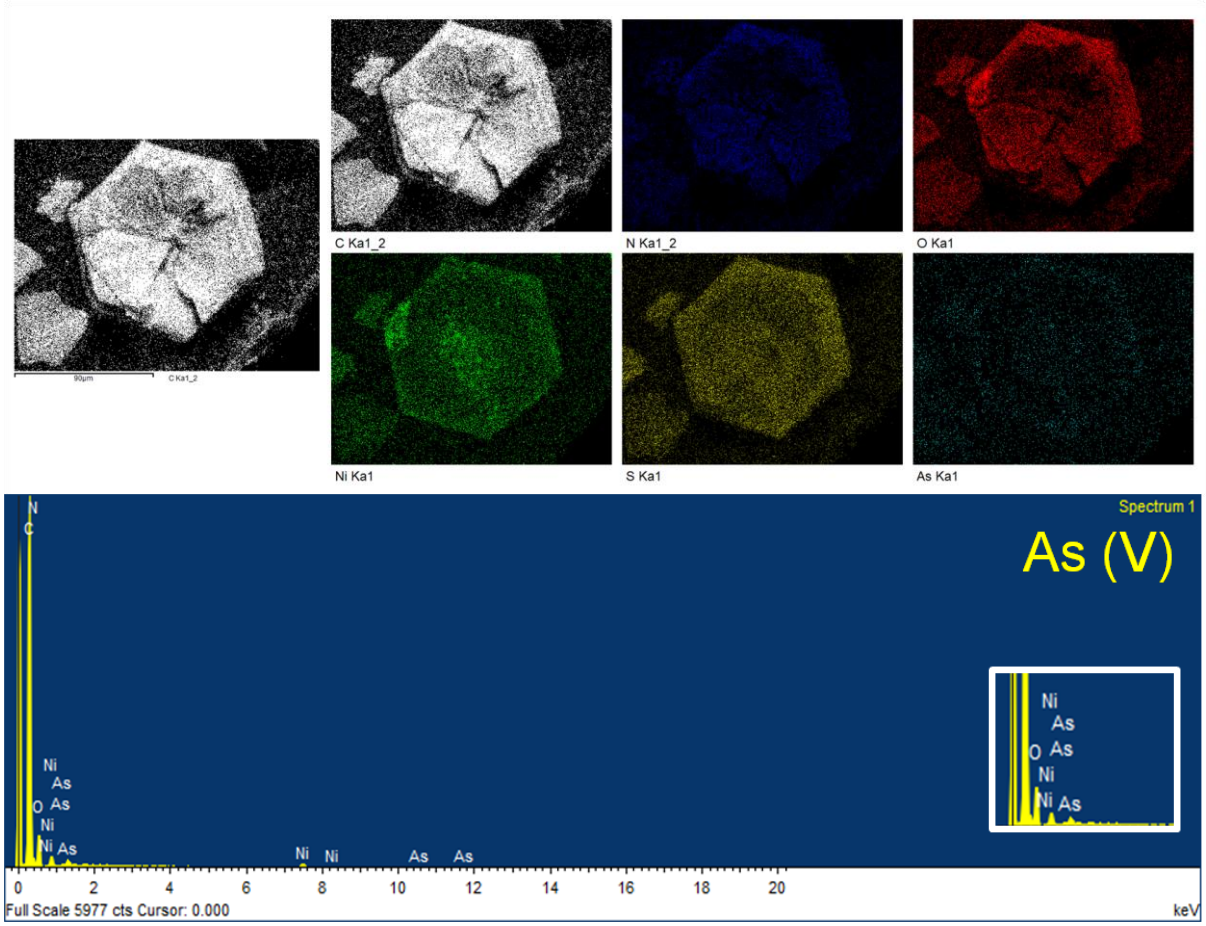

Element	Atomic %
C	63.53
N	17.25
O	16.83
S	0.81
Ni	0.99
As	0.60

Figure S21: EDX mapping profile and spectra for pristine MOF exposed to an aqueous solution of $HAsO_4^{2-}$.

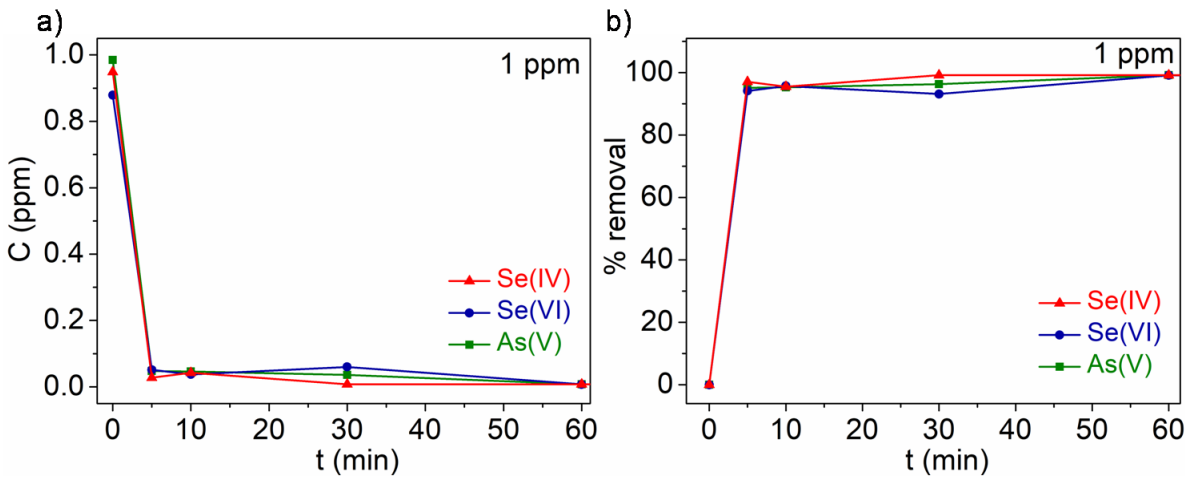

Figure S22: Kinetic profiles of iMOF-3C towards of oxo-anion of Se(IV), Se(VI), As(V) at 1 ppm. (a) Concentration of Se(IV), Se(VI), As(V) as a function of time. (b) % removal plot as a function of time.

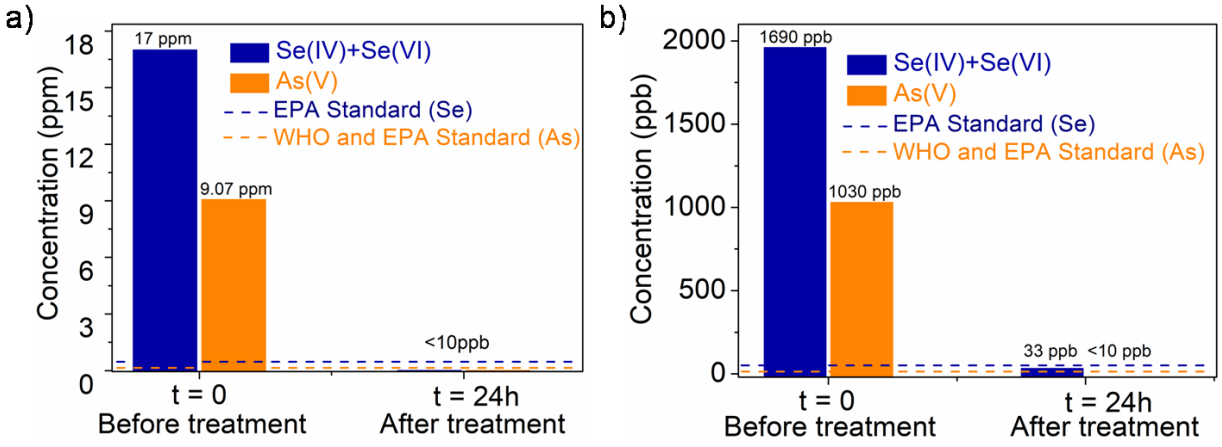

Figure S23: Bar diagram depicting removal of mixture of oxo-anions of Se(IV)/Se(VI)/As(V) at (a) High concentration ~10 ppm. (b) Low concentration ~1000 ppb.

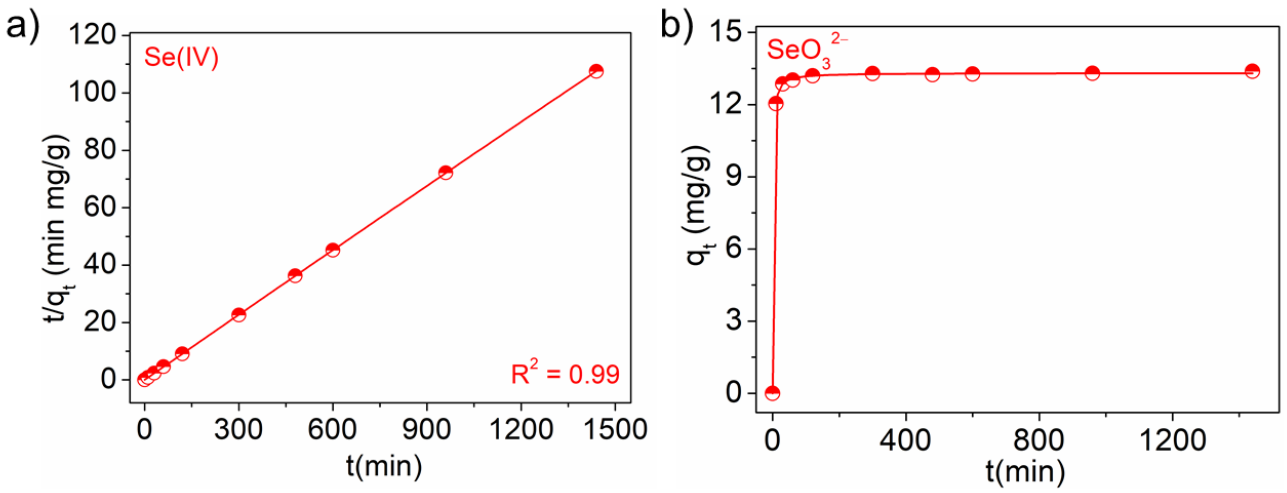

Figure S24: Kinetic profiles of iMOF-3C towards of oxo-anion of Se(IV) at 10 ppm. (a) Pseudo-second order fitting model. (b) Sorption capacity with respect to time.

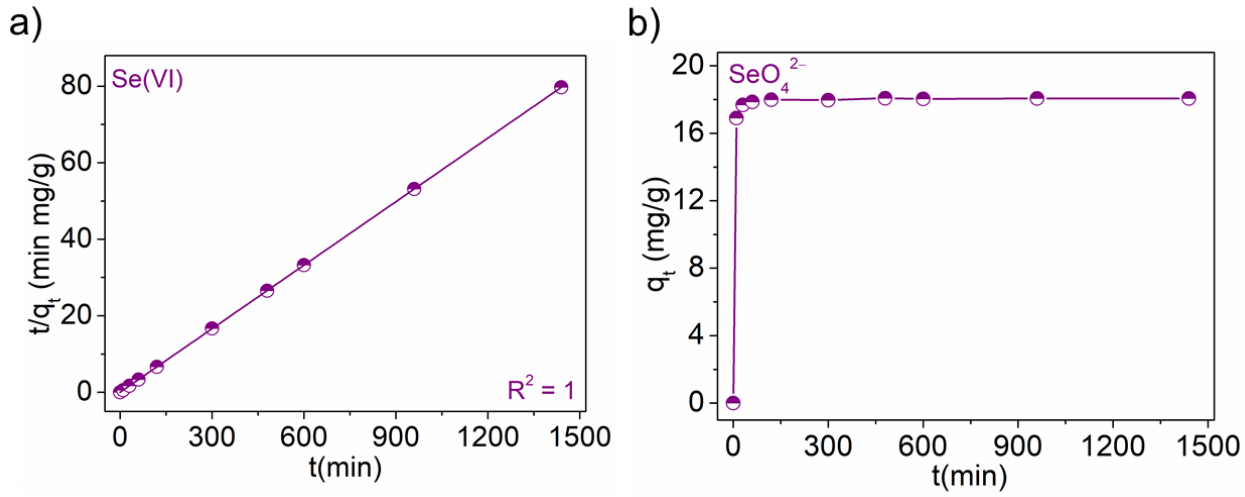

Figure S25: Kinetic profiles of iMOF-3C towards of oxo-anion of Se(VI) at 10 ppm. (a) Pseudo-second order fitting model. (b) Sorption capacity with respect to time.

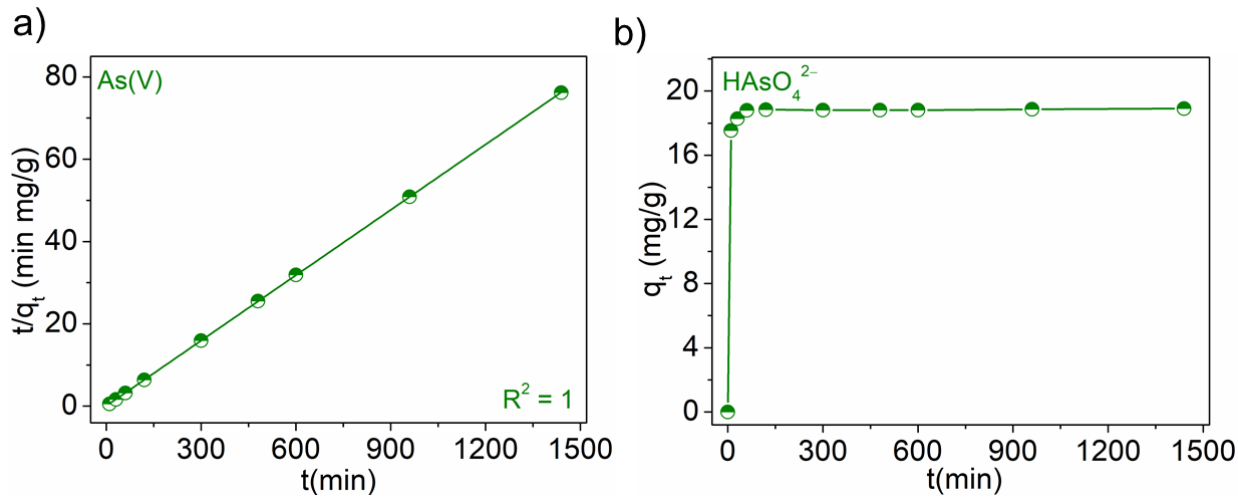

Figure S26: Kinetic profiles of iMOF-3C towards of oxo-anion of As(V) at 10 ppm. (a) Pseudo-second order fitting model. (b) Sorption capacity with respect to time.

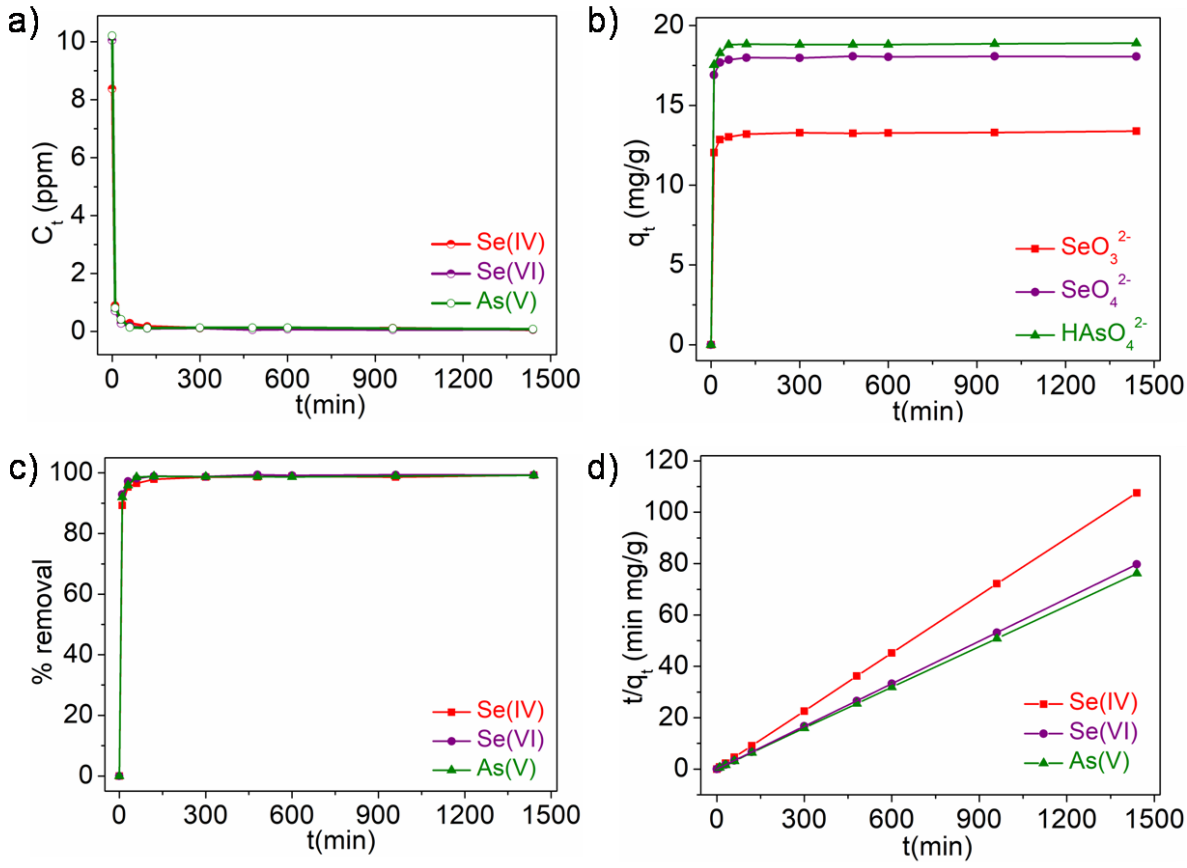

Figure S27: Comparative Kinetic profiles of iMOF-3C towards of oxo-anion of Se(VI), Se(IV), As(V) at 10 ppm. (a) Change in concentration of oxo-anions as a function of time. (b) Sorption capacity with respect to time. (c) % removal plot as a function of time. (d) Pseudo-second order fitting model.

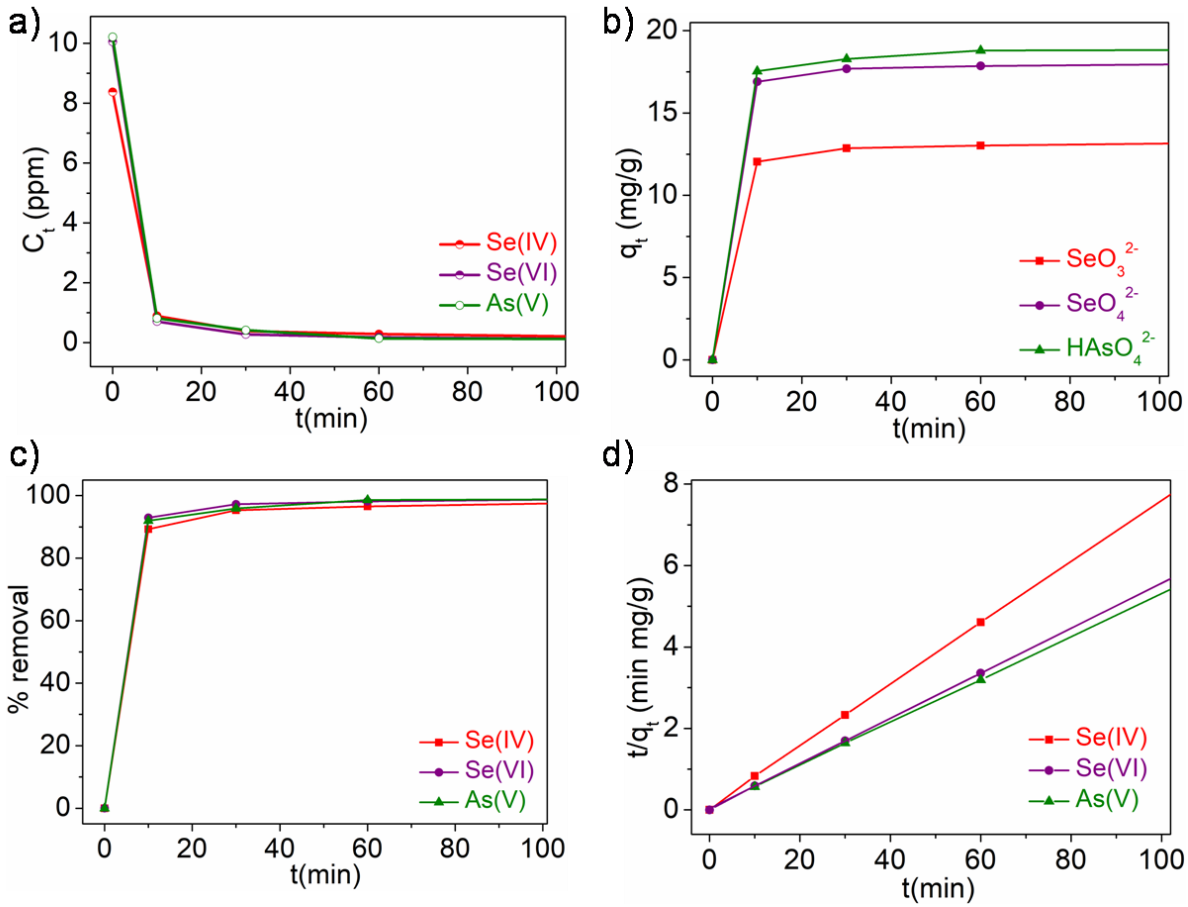

Figure S28: Zoomed View of Comparative Kinetic profiles of iMOF-3C towards of oxo-anion of Se(VI), Se(IV), As(V) at 10 ppm. (a) Change in concentration of oxo-anions as a function of time. (b) Sorption capacity with respect to time (c) .% removal plot as a function of time. (d) Pseudo-second order fitting model.

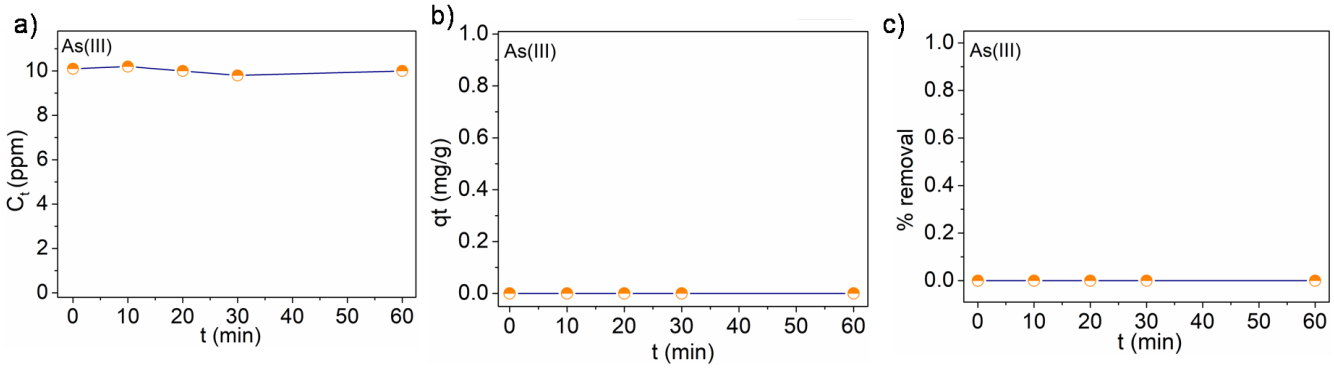

Figure S29: Kinetic profiles of iMOF-3C towards of oxo-anion of As(III). (a) Concentration of As(III) as a function of time. (b) Sorption capacity with respect to time. (c) % removal plot as a function of time (y-axis is divided by 100).

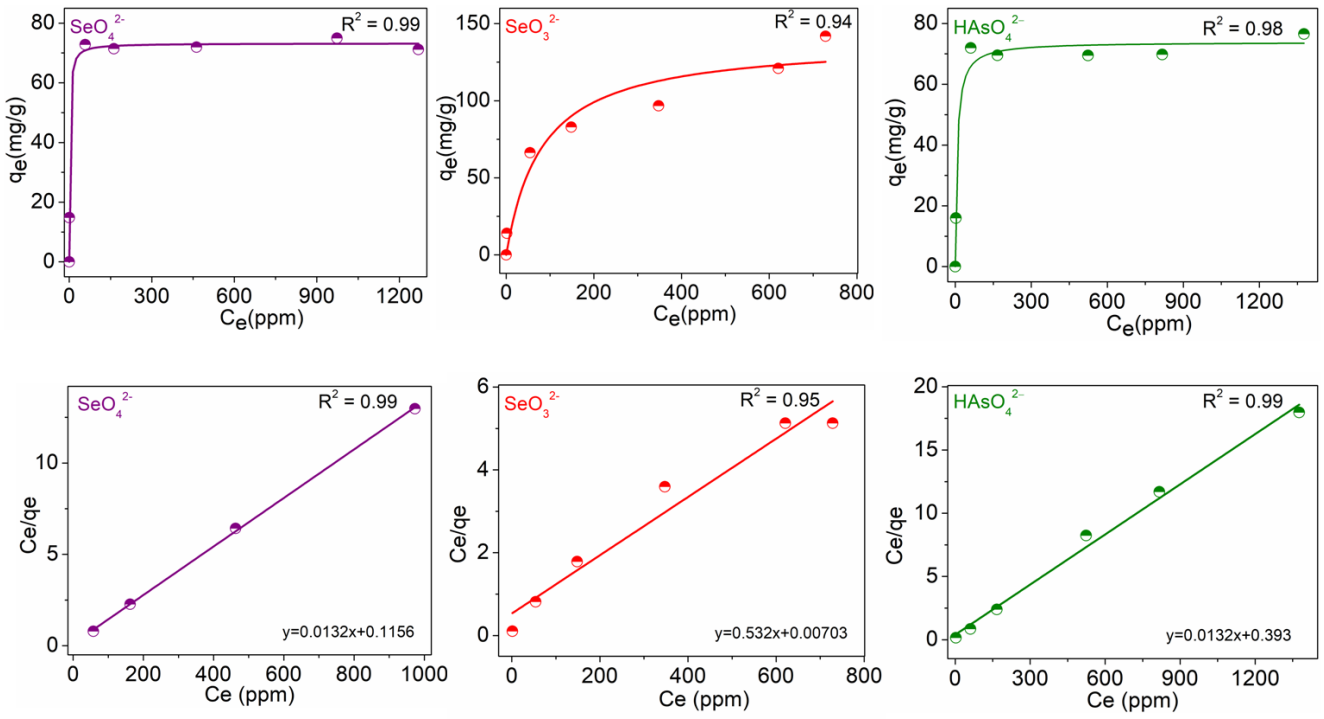

Figure S30: Concentration dependent sorption profiles of iMOF-3C towards of oxo-anion of Se(VI), Se(IV), As(V) and corresponding Langmuir linear fitting model.

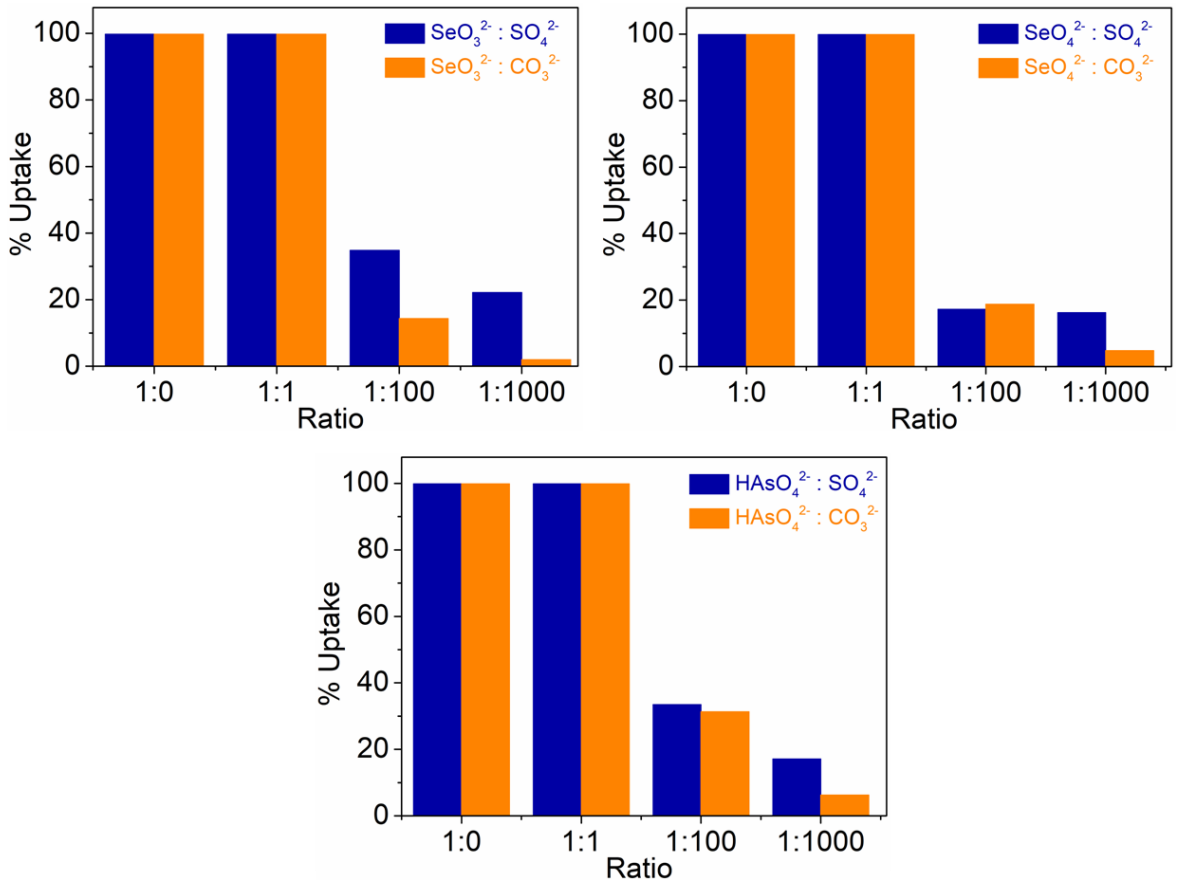

Figure S31: Comparative uptake profiles for capture of oxo-anions viz. Se(IV)/Se(VI)/As(V) in presence of higher concentration of competing ions.

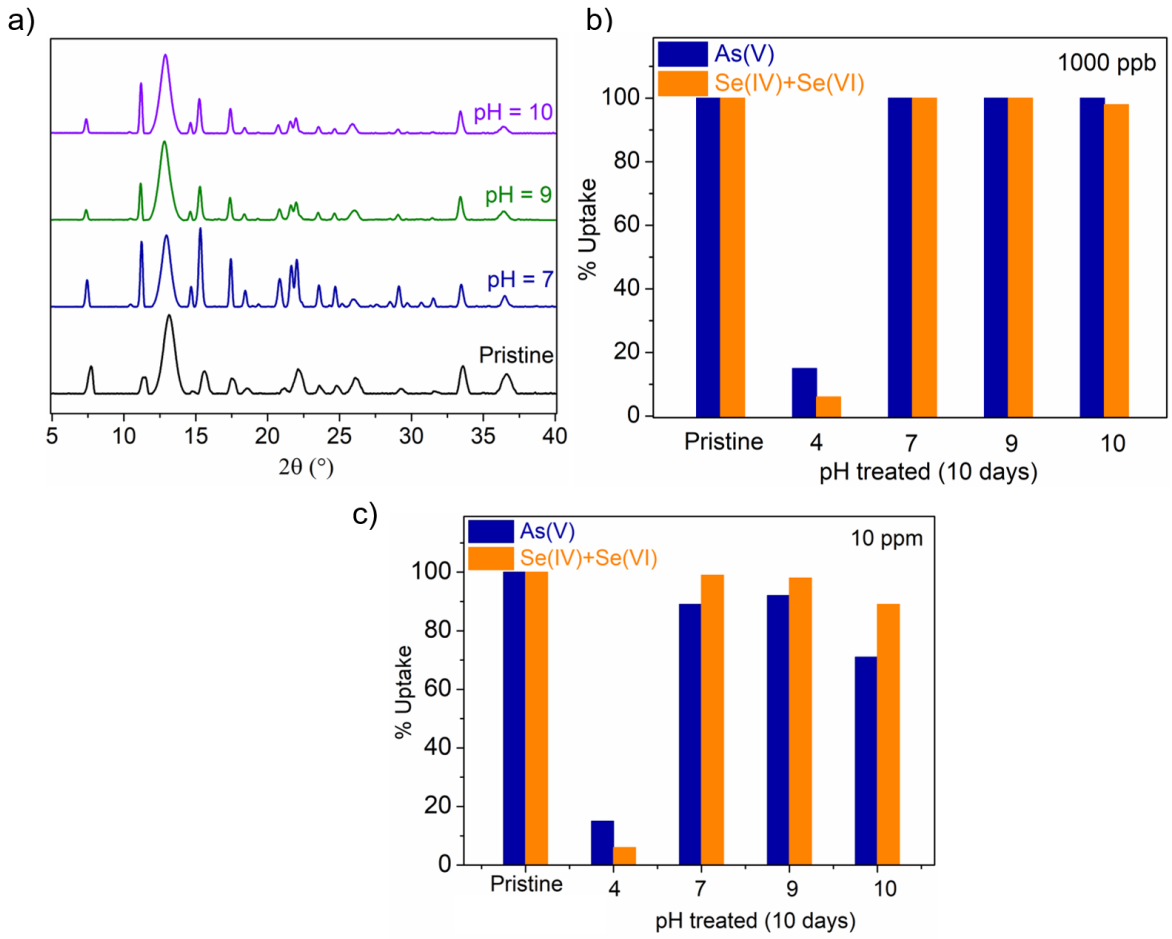

Figure S32: (a) PXRD profiles for iMOF-3C dipped in various pH for 10 days and pristine phase (without treatment). (b), (c) Comparative uptake profiles for capture of oxo-anions of Se(IV)+Se(VI)+As(V) at different pH and concentrations (~1000 ppb and ~10 ppm each) by iMOF-3C with pristine phase (without treatment)

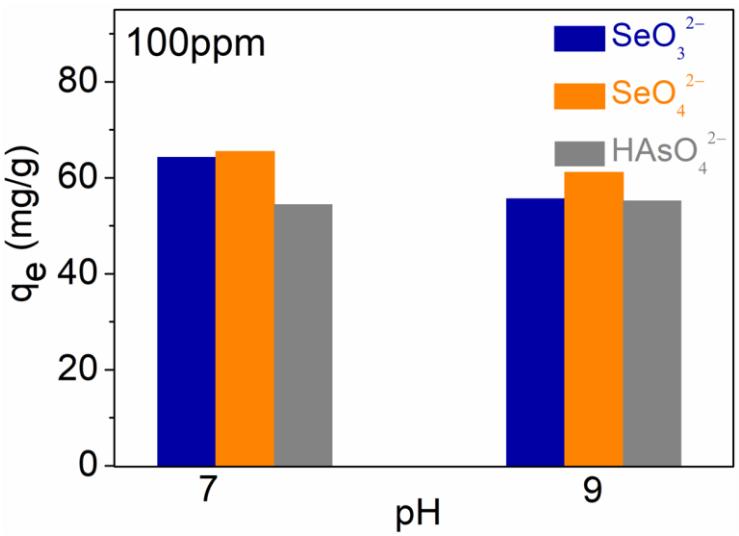

Figure S33: Comparative uptake profiles for capture of oxo-anions viz. Se(IV)/Se(VI)/As(V) at different pH by iMOF-3C.

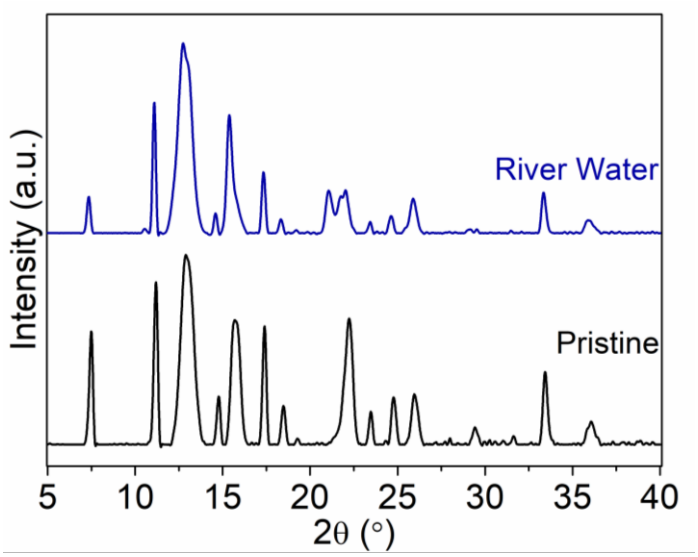

Figure S34: Comparative PXRD spectra for pristine iMOF-3C dipped in River Water.

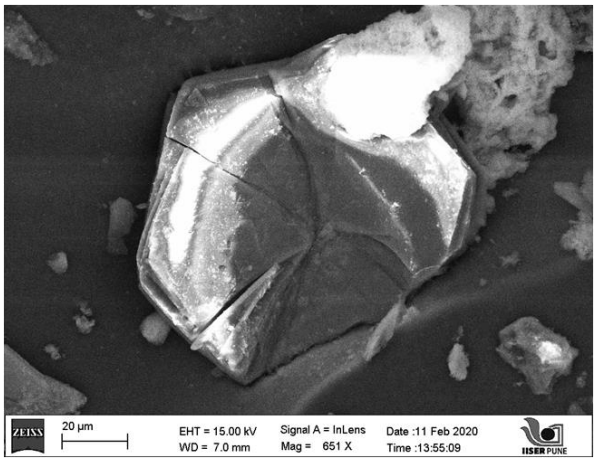

Figure S35: FESEM spectra for pristine iMOF-3C dipped in River Water.

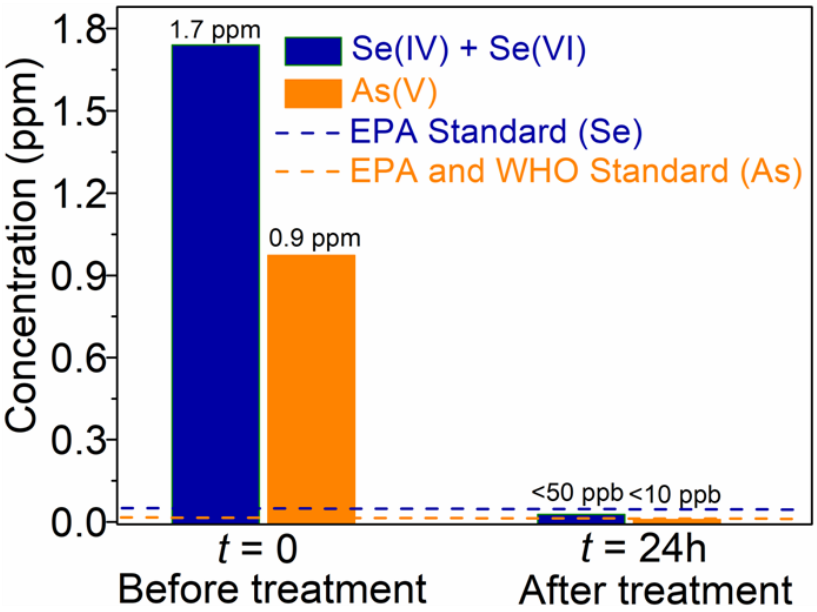

Figure S36: Bar diagram depicting removal of mixture of oxo-anions of Se(IV)/Se(VI)/As(V) at ~1000 ppb in river water.

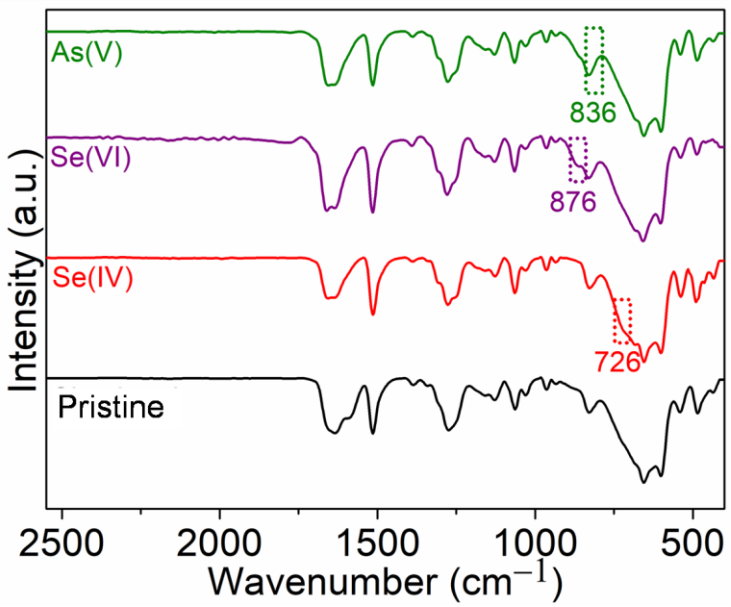

Figure S37: FT-IR spectra for pristine MOF exposed to an aqueous solution of oxo-anions viz. SeO_3^{2-}, SeO_4^{2-}, $HAsO_4^{2-}$.

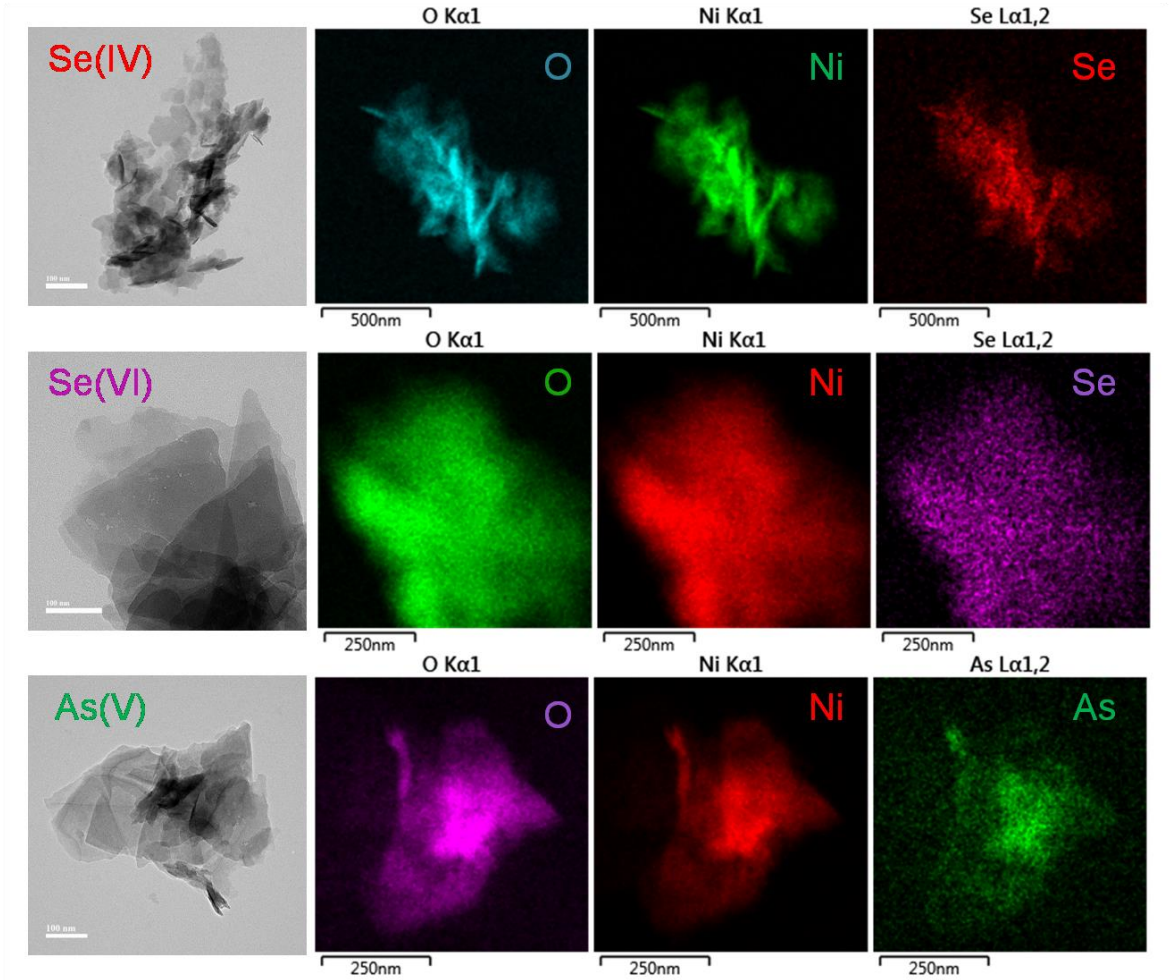

Figure S38: TEM images and TEM-EDS spectra for pristine MOF exposed to an aqueous solution of SeO_3^{2-}. SeO_4^{2-}, $HAsO_4^{2-}$ (1000ppm).

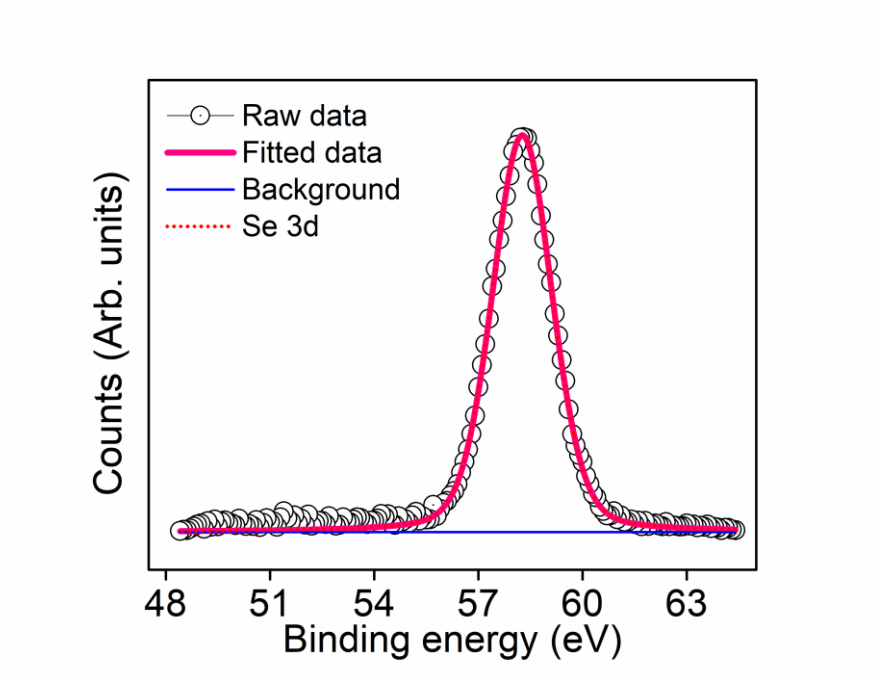

Figure S39: XPS spectra for pristine MOF exposed to an aqueous solution of oxo-anions viz. SeO_3^{2}.

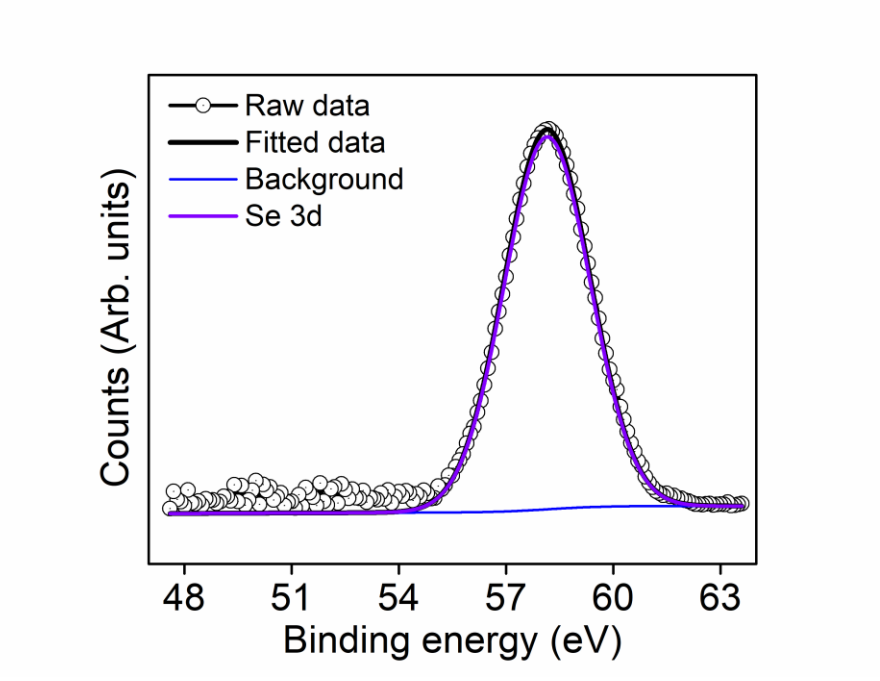

Figure S40: XPS spectra for pristine MOF exposed to an aqueous solution of oxo-anions viz. SeO_4^{2-}.

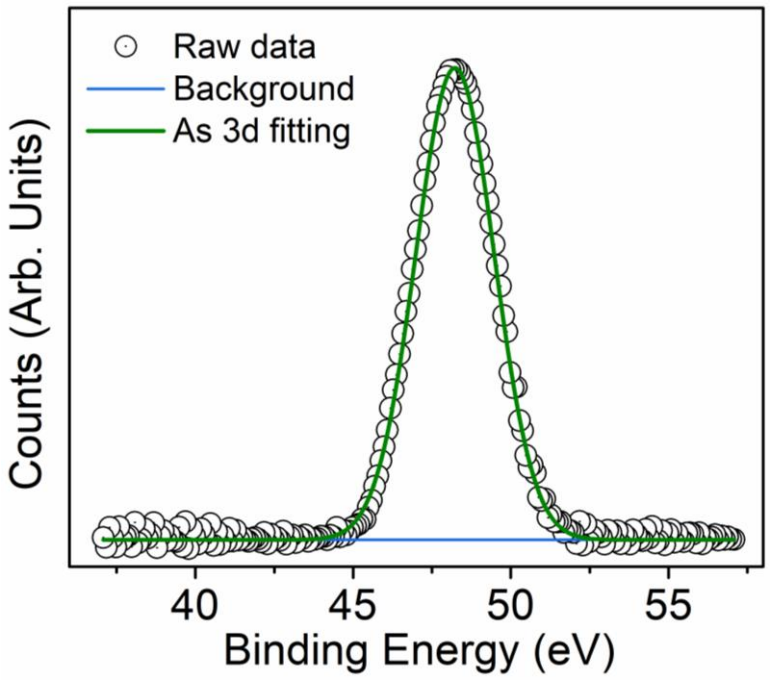

Figure S41: XPS spectra for pristine MOF exposed to an aqueous solution of oxo-anions viz. $HAsO_4^{2-}$.

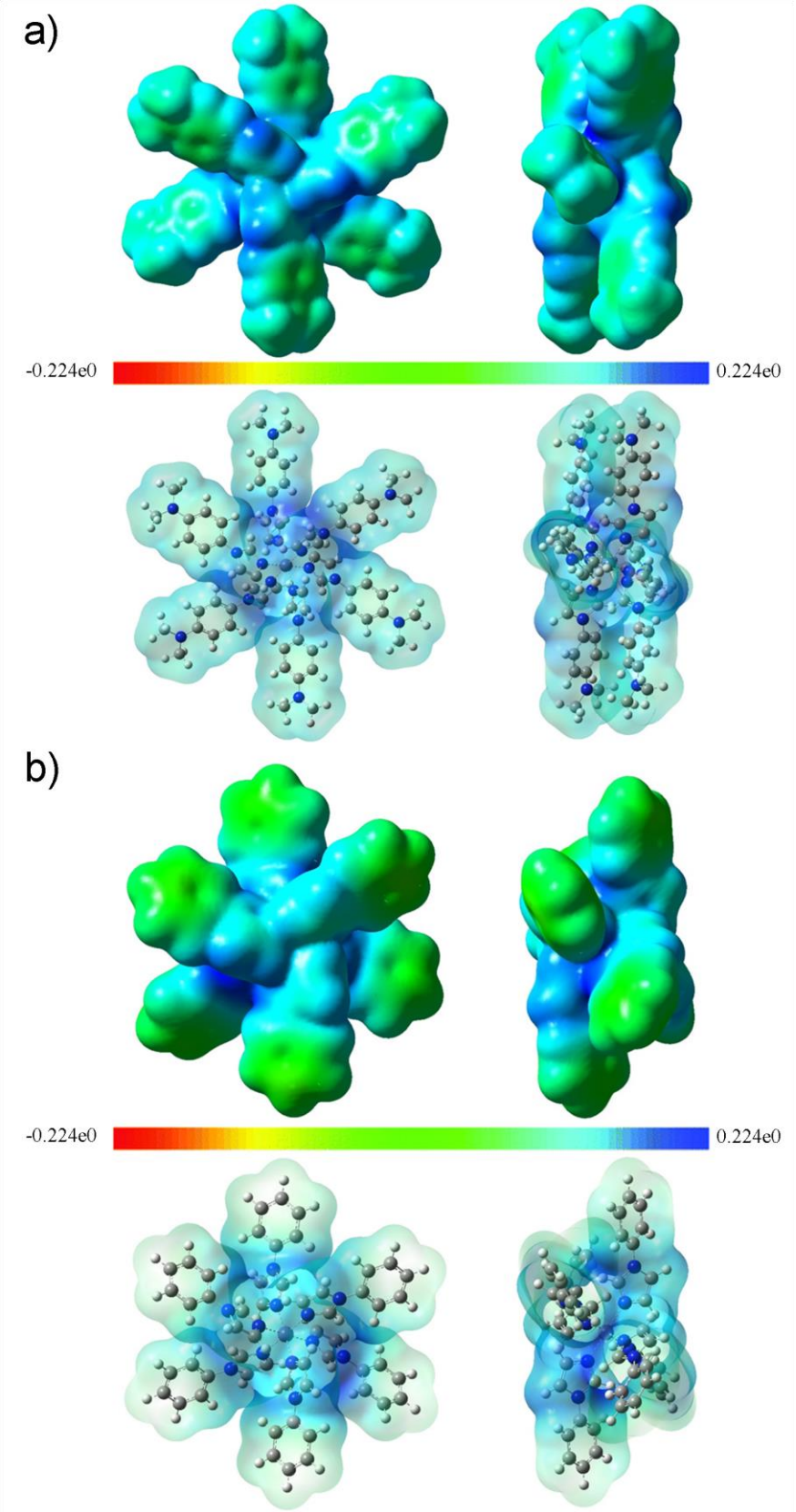

Figure S42: Electrostatic Potential (ESP) diagram of two different part of framework in iMOF-3C.

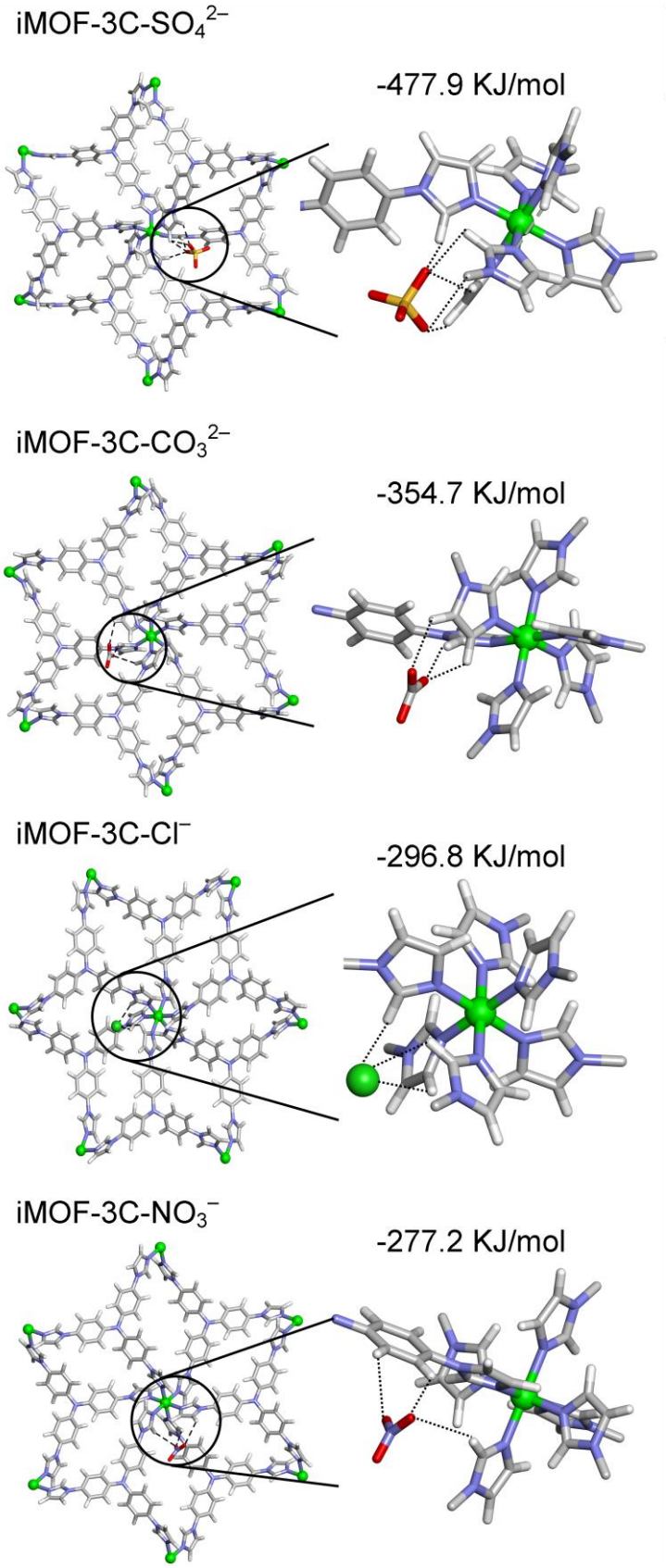

Figure S43: Optimized structures and corresponding zoomed view showing hydrogen bonding interactions of iMOF-3C with different anions and binding energies.

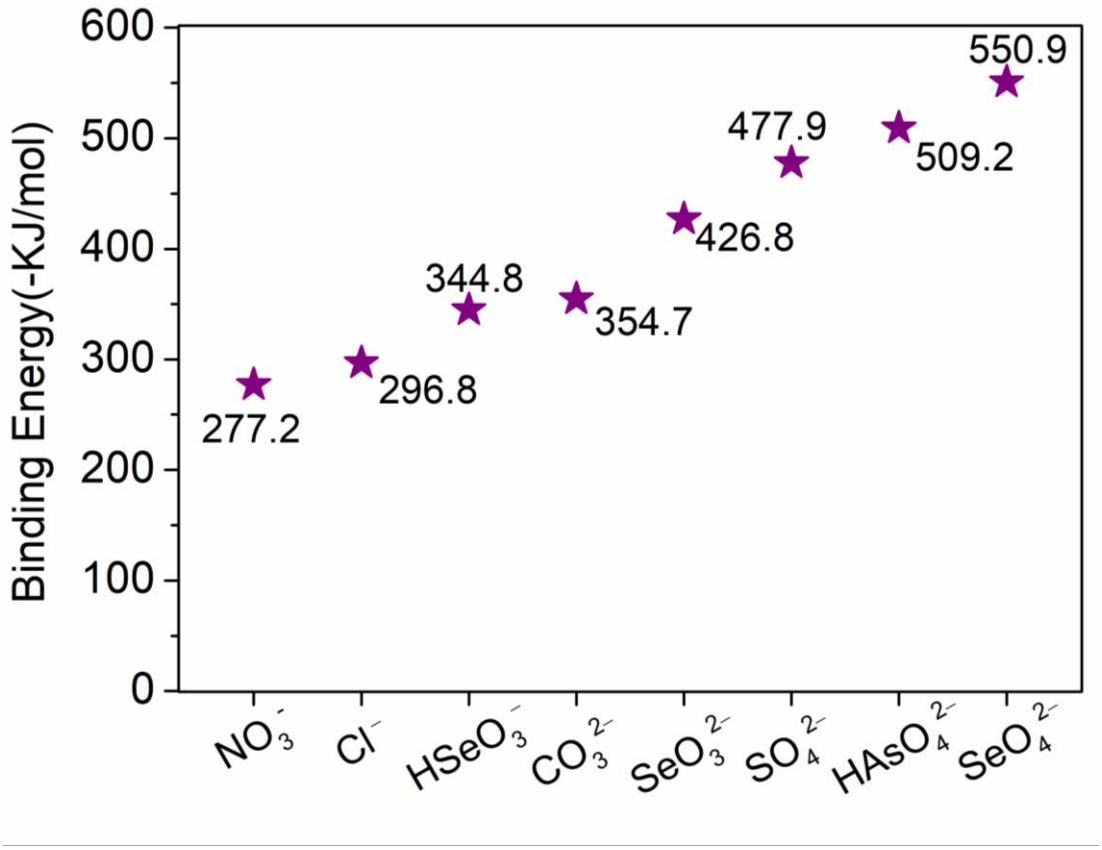

Figure S44: Static binding energies for various anions in iMOF-3C framework calculated using density functional theory (DFT).

Table S1: Comparison of unit-cell parameters for pristine iMOF-3C and corresponding anion exchanged products viz. iMOF-3C-SeO_3^{2-}, iMOF-3C-SeO_4^{2-}, iMOF-3C-$HAsO_4^{2-}$.

Unit cell parameters	iMOF-C3	iMOF-C3-SeO_3^{2-}	iMOF-C3-SeO_4^{2-}	iMOF-C3-$HAsO_4^{2-}$
a (Å)	16.01(3)	16.06(5)	15.97(3)	16.06(6)
b (Å)	16.01(3)	16.06(5)	15.97(3)	16.06(6)
c (Å)	25.63(5)	25.79(7)	25.97(7)	24.79(8)
$\alpha^{(o)}$	90	90	90	90
$\beta^{(o)}$	90	90	90	90
$\gamma^{(o)}$	120	120	120	120
Volume ($Å^3$)	5691(2)	5967(30)	5550(20)	5540(30)

Table S2: Concentration of Ni(II) ion in the supernatant of various media as recorded by ICP-MS.

pH	Concentration of Ni (ppm)	
	1 day	10 days
4	-	> 400
7	0.48	0.28
9	0.54	0.1
10	0.18	0.4

Table S3: Concentration of Ni(II) ion in the supernatant of iMOF-3C exposed to toxic oxo-anions of Se(IV)/Se(VI)/As(V)/As(III) as recorded by ICP-MS.

	Concentration of Ni (ppm)
Se(IV)	N.D.
Se(VI)	0.27
As(V)	0.26
As(III)	0.51

Table S4: Sorption kinetics data for uptake of Se(IV) by iMOF-3C at low concentration.

C_o(ppm) Se(IV)	Time(min)	C_f	Removal (%)	K_d (mL/g)	q_t (SeO_3^{2-}) (mg/g)
8.37	10	0.895	89.31	8.4×10^3	12.04
	30	0.388	95.36	2.0×10^4	12.86
	60	0.287	96.57	2.8×10^4	13.02
	120	0.177	97.88	4.6×10^4	13.20
	300	0.118	98.59	6.9×10^4	13.28
	480	0.11	98.68	7.5×10^4	13.24
	600	0.0925	98.89	8.9×10^4	13.27
	960	0.116	98.61	7.1×10^4	13.29
	1440	0.06	99.28	1.3×10^5	13.38
	1800	<10ppb	>99.40	$>8.3 \times 10^5$	>13.38

Table S5: Kinetics Sorption kinetics data for uptake of Se(VI) by iMOF-3C at low concentration.

C_o (ppm) Se(VI)	Time(min)	C_f	Removal (%)	K_d (mL/g)	q_t (SeO_4^{2-}) (mg/g)
10.05	10	0.71	92.93	1.3×10^4	16.9
	30	0.28	97.23	3.5×10^4	17.68
	60	0.18	98.19	5.4×10^4	17.86
	120	0.10	98.91	9.1×10^4	17.99
	300	0.12	98.8	8.2×10^4	17.97
	480	0.06	99.39	1.63×10^5	18.08
	600	0.08	99.19	1.22×10^5	18.04
	960	0.06	99.37	1.56×10^5	18.07
	1440	0.07	99.3	1.42×10^5	18.06
	1800	<10ppb	>99.90	1.0×10^6	>18.17

Table S6: Sorption kinetics data for uptake of As(V) by iMOF-3C at low concentration.

C_o (ppm) As(V)	Time(min)	C_f	Removal (%)	K_d (mL/g)	q_t ($HAsO_4^{2-}$) (mg/g)
10.21	10	0.81	92.01	1.1×10^4	17.54
	30	0.42	95.9	2.3×10^4	18.28
	60	0.14	98.62	7.1×10^4	18.8
	120	0.12	98.84	8.5×10^4	18.84
	300	0.13	98.71	7.7×10^4	18.81
	480	0.13	98.72	7.7×10^4	18.81
	600	0.13	98.7	7.7×10^4	18.81
	960	0.11	98.94	9.3×10^4	18.86
	1440	0.083	99.18	1.22×10^5	18.91
	1800	<10ppb	>99.90	1.02×10^6	>19.04

Table S7: Uptake performance of iMOF-3C towards oxo-anion of Se(IV)+Se(VI), As(V) at 10ppm.

	C_o (ppm)	C_f (ppm)	% removal	K_d (mL/g)
Se(IV) + Se(VI)	17	<10ppb	>99.94	$>1.6 \times 10^6$
As(V)	9.07	<10ppb	>99.8	$> 0.9 \times 10^6$

Table S8: Listing kinetic fitting parameters as obtained by pseudo-second order fitting model for oxo-anions of Se(IV)/Se(VI)/As(V) by iMOF-3C.

	q_e (exp.) mg/g	q_e (cal.) mg/g	k_2	R^2
Se(IV)	13.38	13.37	0.039	0.99
Se(VI)	18.06	18.08	0.093	1
As(V)	18.9	18.89	0.057	1

Table S9: Comparative analysis of static binding energies in iMOF-3C framework calculated using density functional theory (DFT) and hydration energy from literature values.

Anion	Cl^-	NO_3^-	CO_3^{2-}	SO_4^{2-}	SeO_4^{2-}	SeO_3^{2-}	$HSeO_3^-$	$HAsO_4^{2-}$
Binding energy (-KJ/mol)	296.89	277.29	354.7	477.9	550.9	426.8	344.8	509.2
Hydration Energy (-KJ/mol)	340	300	1315	1080	900	937-1025	NA	NA
Reference	25	25	25	25	25	26	-	-

Table S10: Comparison for state-of-the-art materials available for capture of Se(IV) oxo-anion.

Adsorbent	Oxo-anion	Method	Selectivity	Capacity (mg/g)	Time (min)	Reference
iMOF-3C	Se(IV)	Ion-exchange	vs. NO_3^-, Cl^-, CO_3^{2-}, SO_4^{2-}	140	5	This work
NU-1000	Se(IV)	Adsorption	NA	95	1	2
CAU-17	Se(IV)	Irreversible Chemical Bond	vs. CO_3^{2-}, Cl^-, NO_3^-, SO_4^{2-} etc	255.3	360	27
MgAl-MoS4-LDH	Se(IV)	Ion-exchange	NA	294	10	3
LDH	Se(IV)	Ion-exchange	vs. CO_3^{2-}, Cl^-, NO_3^-, HPO_4^{2-}, SO_4^{2-}	207	100	28
MgO Nanosheets	Se(IV)	Adsorption	NO_3^-, Cl^-, F^-, PO_4^{3-}	103.52	300	29
Iron Oxide on SiO_2	Se(IV)	Adsorption	NA	20.4	120	30

Table S11: Comparison for state-of-the-art materials available for capture of Se(VI) oxo-anion.

Adsorbent	Oxo-anion	Method	Selectivity	Capacity (mg/g)	Time (min)	Reference
iMOF-3C	Se(VI)	Ion-exchange	vs. NO_3^-, Cl^-, CO_3^{2-},SO_4^{2-}	73	5	This work
iMOF-1C	Se(VI)	Ion-exchange	vs. NO_3^-, Cl^-, SO_4^{2-}, HCO_3^-, CO_3^{2-}	100	4320	1
NU-1000	Se(VI)	Adsorption	NA	85	1	2
CAU-17	Se(VI)	Irreversible Chemical Bond	vs. NO_3^-, NO_2^-, SO_4^{2-}, F^-, Cl^-, HCO_3^- ,CO_3^{2-}, Ac^-, PO_4^{3-}, LAS^-, $B_4O_7^{2-}$	20.3	600	27
MOF-808	Se(VI)	Adsorption	NA	118	5	31
MgAl-MoS4-LDH	Se(VI)	Ion-exchange	NA	85	30	3
MgO Nanosheets	Se(VI)	Adsorption	NO_3^-, Cl^-, F^-, PO_4^{3-}	10.28	300	29
Iron oxide on chitosan	Se(VI)	Adsorption	vs. SO_4^{2-}	17	1440	32
Cu^{2+}-anchored diamino functionalized MCM-41	Se(VI)	Adsorption	vs SO_4^{2-}	83	600	33
Polyamine-type ion-exchange resin	Se(VI)	Adsorption	vs. SO_4^{2-}, Cl^-	243	180	34

Table S12: Comparison for state-of-the-art materials available for capture of As(V) oxo-anion.

Adsorbent	**Oxo-anion**	**Method**	**Selectivity**	**Capacity (mg/g)**	**Time (min)**	**Reference**
iMOF-3C	As(V)	Ion-exchange	vs. NO_3^-, Cl^-, CO_3^{2-}, SO_4^{2-}	75.5	5	This work
iMOF-1C	As(V)	Ion-exchange	vs. NO_3^-, Cl^-, CO_3^{2-}, HCO_3^- , SO_4^{2-}	85	4320	1
UiO-66	As(V)	Adsorption	NA	303 at pH=2	2880	35
Mg/Al-LDH	As(V)	Ion-exchange	vs. SO_4^{2-}, NO_3^-, Cl^-	56	5	36
Fe-BTC	As(V)	Adsorption	NA	12.3	10	37
MIL-53(Al)	As(V)	Adsorption	vs. CO_3^{2-}, Cl^-, NO_3^-, SO_4^{2-}	106.5	660	38
MIL-53(Fe)	As(V)	Adsorption	NA	21.27	90	38
ZIF-8 (prepared in MeOH)	As(V)	Adsorption	NA	72.33	90	39

Table S13. Crystal data and structure refinement for iMOF-3C

Identification code	iMOF-3C (CCDC - 1990643)	
Empirical formula	C54 H42 N14 Ni	
Formula weight	945.72	
Temperature	150(2) K	
Wavelength	0.71073 Å	
Crystal system	Trigonal	
Space group	R- 3: H	
Unit cell dimensions	a = 16.012(3) Å	α= 90°.
	b = 16.012(3) Å	β= 90°.
	c = 25.633(5) Å	γ = 120°.
Volume	5691(2) $Å^3$	
Z	3	
Density (calculated)	0.828 mg/m^3	
Absorption coefficient	0.289 mm^{-1}	
F(000)	1476	
Crystal size	0.13 x 0.12 x 0.10 mm^3	
Theta range for data collection	2.384 to 28.368°.	
Index ranges	-21<=h<=21, -21<=k<=21, -34<=l<=29	
Reflections collected	30467	
Independent reflections	3159 [R(int) = 0.123]	
Completeness to theta = 25.242°	99.9 %	
Refinement method	Full-matrix least-squares on F^2	
Data / restraints / parameters	3159 / 0 / 105	
Goodness-of-fit on F^2	0.907	
Final R indices [I>2sigma(I)]	R1 = 0.07, wR2 = 0.26	
Extinction coefficient	n/a	
Largest diff. peak and hole	2.246 and -0.779 e.$Å^{-3}$	

References

(1) S. Sharma, A. V. Desai, B. Joarder and S. K. Ghosh, *Angew. Chem.* 2020, **59**, 7788-7792.

(2) A. J. Howarth, M. J. Katz, T. C. Wang, A. E. Platero-Prats, K.W. Chapman, J. T. Hupp and O. K. Farha, J. *Am. Chem. Soc.*, 2015, **137**, 23, 7488-7494.

(3) L. Ma, S. M. Islam, C. Xiao, J. Zhao, H. Liu, M. Yuan, G. Sun, H. Li, S. Ma and M. G. Kanatzidis *J. Am. Chem. Soc.*, 2017, **139**, 12745−12757.

(4) SAINT Plus, Bruker AXS Inc.: Madison, WI, 2004.

(5) L. Krause, R. Herbst-Irmer, G. M. Sheldrick, D. *J.* Stalke, *Appl. Cryst.*, 2015, **48**, 3-10.

(6) G. M. Sheldrick, SHELXTL, Reference Manual, version 5.1; Bruker AXS Inc.:Madison, WI, 1997.

(7) G. M. Sheldrick, *Acta. Cryst.*, 2008, ***A64***, 112-122.

(8) G. M. Sheldrick, *Acta. Cryst.*, 2015, **C71**, 3-8.

(9) L. Farrugia, WinGX, 2009, University of Glasgow: Glasgow, Scotland.

(10) A. L. Spek, *Acta. Cryst.*, 2015, **C71**, 9-18.

(11) G. Kresse and *J.* Hafner, *Phys. Rev. B*, 1993, **48**, 13115-13118.

(12) S. Grimme, S. Ehrlich and L. Goerigk, *J. Comp. Chem.*, 2011, **32**, 1456-1465.

(13) J. P. Perdew, K. Burke and M. Ernzerhof, *Phys. Rev. Lett.*, 1996, **77**, 3865-3868.

(14) G. Kresse and D. Joubert, *Phys. Rev. B*, 1999, **59**, 1758-1775.

(15) Gaussian 09, Revision E.01, M. J. Frisch, G. W. Trucks, H. B. Schlegel, G. E. Scuseria, M. A. Robb, J. R. Cheeseman, G. Scalmani, V. Barone, B. Mennucci, G. A. Petersson, H. Nakat-suji, M. Caricato, X. Li, H. P. Hratchian, A. F. Izmaylov, J. Bloino, G. Zheng, J. L. Sonnenberg, M. Hada, M. Ehara, K. Toyota, R. Fukuda, J. Hasegawa, M. Ishida, T. Nakajima, Y. Honda, O. Kitao, H. Nakai, T. Vreven, J. A. Montgomery Jr., J. E. Peralta, F. Ogliaro, M. Bearpark, J. J. Heyd, E. Brothers, K. N. Kudin, V. N. Staroverov, R. Kobayashi, J. Normand, K. Raghavachari, A. Rendell, J. C. Burant, S. S. Iyengar, J. Tomasi, M. Cossi, N. Rega, J. M. Millam, M. Klene, J. E. Knox, J. B. Cross, V. Bakken, C. Adamo, J. Jaramillo, R. Gomperts, R. E. Stratmann, O. Yazyev, A. J. Austin, R. Cammi, C. Pomelli, J. W .Ochterski, R. L. Martin, K. Morokuma, V. G. Zakrzewski, G. A. Voth, P. Salvador, J. J. Dannenberg, S. Dapprich, A. D. Daniels, Ö.Farkas, J. B. Foresman, J. V. Ortiz, J. Cioslowski and D. J. Gaussian Fox, , Inc., Wallingford CT, 2009.

(16) A. V. Marenich, C. J. Cramer and D. G. Truhlar, *J. Phys. Chem. B.*, 2009, **113**, 6378-6396.

(17) A. D. Becke, *J. Chem. Phys.*, 1993, **98**, 5648-5652.

(18) C. T. Lee, W. T. Yang and R. G. Parr, *Phys. Rev. B.*, 1988, **37**, 785-789.

(19) S. Grimme, J. Antony, S. Ehrlich and H. *J.* Krieg, *Chem. Phys.*, 2010, **132**, 154104-154123.

(20) M. Dolg, U. Wedig, H. Stoll, and H. J. Preuss, *Chem. Phys.*, 1987, **86**, 866-872.

(21) D. Andrae, U. Haeussermann, M. Dolg, H. Stoll and H. Preuss, *Theor. Chim. Acta*, 1990, **77**, 123-141.

(22) W. J. Hehre, R. Ditchfie, and J. A. Pople, *J. Chem. Phys.*, 1972, ***56***, 2257-2261.

(23) Dassault Systèmes BIOVIA, Material Studio, San Diego: Dassault Systèmes, 2019.

(24) A. K. Rappe, C. J. Casewit, K. S. Colwell, W. A. Goddard and W. M. Skiff, *J. Am. Chem. Soc.*, 1992, **114**, 10024-10035.

(25) Y. Marcus, *J. Chem. Soc. Faraday Trans.*, 1991, **87**, 2995-2999.

(26) A. Meleshyn and H. Wicke, *J. Phys. Chem. A*, 2010, **114**, 8948–8960.

(27) H. Ouyang, N. Chen, G. Chang, X. Zhao, Y. Sun, S. Chen, H. Zhang and D. Yang, Angew. *Chem. Int. Ed.*, 2018, **57**, 13197– 13201.

(28) L. Zhu, L. Zhang, J. Li, D. Zhang, L. Chen, D. Sheng, S. Yang, C. Xiao, J. Wang, Z. Chai, T. E. Albrecht-Schmitt and S. Wang, *Environ. Sci. Technol.*, 2017, **51**, 8606−8615.

(29) W. Cui, P. Li, Z. Wang, S. Zheng and Y. Zhanga, *J. Hazard. Mat.*, 2018, **341**, 268-276.

(30) Y. T. Chana, W. H. Kuanb, T. Y. Chenc and M. K. Wanga, *Water Res.*, 2009, **43**, 4412–4420.

(31) R. J. Drout, A. J. Howarth, K. -i. Otake, T. Islamoglu and O. K. Farha, *CrystEngComm*, 2018, **20**, 6140.

(32) N. Bleiman and Y. G. Mishael, *J. Hazard. Mat.*, 2010, **183**, 590-595.

(33) T. Yokoi, T. Tatsumi, and H. Yoshitake, *Bull. Chem. Soc. Jpn*., 2003, **76**, 2225–2232.

(34) H. Hashimoto, M. Nakayama and T. Nishimura, *Sep. Sci. Technol.*, 2007, **42**, 3155–3167.

(35) C. Wang, X. Liu, J. P. Chen and K. Li, *Sci. Rep.*, 2015, DOI: 10.1038/srep16613.

(36) L. Ma, S. M. Islam, H. Liu, J. Zhao, G. Sun, H. Li, S. Ma and M. G. Kanatzidis, *Chem. Mater.*, 2017, **29**, 3274-3284.

(37) B. J. Zhu, X. Y. Yu, Y. Jia, F. M. Peng, B. Sun, M.-Y. Zhang, T. Luo, J.-H. Liu and X.-J. Huang, J. *Phys. Chem. C*., 2012, **116**, 8601-8607.

(38) J. Li, Y.-n. Wu, Z. Li, M. Zhu and F. Li, *Water Sci. Technol*., 2014, **70**, 1391- 1397.

(39) Y.-n. Wu, M. Zhou, B. Zhang, B. Wu, J. Li, J. Qiao, X. Guan and F. Li, Nanoscale, 2014, **6**, 1105-1112.